Geophysical Journal International

Geophys. J. Int. (2012) **188,** 301–324 doi: 10.1111/j.1365-246X.2011.05261.x

Remote triggering of non-volcanic tremor around Taiwan

Kevin Chao,[1] Zhigang Peng,[1] Chunquan Wu,[1] Chi-Chia Tang[1,2,3] and Cheng-Horng Lin[3]

[1]*School of Earth and Atmospheric Sciences, Georgia Institute of Technology, Atlanta, GA, USA. E-mail: kevinchao@gatech.edu*
[2]*Department of Earth and Environmental Science, National Chung Cheng University, Chia-Yi, Taiwan*
[3]*Institute of Earth Sciences, Academia Sinica, Taipei, Taiwan*

Accepted 2011 October 8. Received 2011 October 3; in original form 2010 December 30

SUMMARY

We perform a systematic survey of triggered deep 'non-volcanic' tremor beneath the Central Range (CR) in Taiwan for 45 teleseismic earthquakes from 1998 to 2009 with $M_w \geq 7.5$ and epicentral distance $\geq$1000 km to the broad-band station TPUB. Triggered tremors are visually identified as bursts of high-frequency (2–8 Hz), non-impulsive and long-duration seismic energy that are coherent among many seismic stations and modulated by the teleseismic surface waves. Out of the 45 earthquakes, we identified nine teleseismic events associated with nine tremor sources in the southern and five in the northern CR. Most of the tremor sources are located within the depth range of 15–25 km in the lower crust above the Moho. We find that the amplitudes of the surface waves play an important role in determining the triggering potential, and the apparent triggering threshold is $\sim$0.1 cm s^{-1}, or 7–8 KPa. However, such threshold is partially controlled by the background noise level, which could prevent weaker tremor triggered by surface waves with smaller amplitudes from being identified. The amplitudes of the triggered tremor show a positive correlation with the amplitudes of the triggering surface waves, consistent with the predictions by the 'clock-advance' model. In addition to amplitudes, other factors, such as frequency contents and incidence angles, also affect the triggering potential. We find that intermediate-period (30–10 s) surface waves could trigger/modulate tremors, suggesting that long-period (>30 s) surface waves are not always required in long-range triggering. Tremors appear to be triggered by both Love and Rayleigh waves. When the incidence angles are parallel to the strike of the CR, all six events triggered tremor primarily during the Rayleigh waves. For strike normal incidence, only the 2001 M_w7.8 Kunlun earthquake showed predominant Love-wave triggering. This observation can be qualitatively explained by a simple Coulomb failure for a left-lateral shear on the low-angle detachment fault beneath the southern CR.

Key words: Earthquake interaction, forecasting, and prediction; Rheology and friction of fault zones; Dynamics and mechanics of faulting.

1 INTRODUCTION

Deep 'non-volcanic' tremor is a newly observed seismic signal away from volcanic regions with non-impulsive arrival, low amplitude and long duration (Schwartz & Rokosky 2007; Peng & Gomberg 2010; Rubinstein *et al.* 2010; Beroza & Ide 2011; and references therein). After the initial discovery of tremor in southwest Japan (Obara 2002), tremors have been identified in many regions along major plate boundaries around the Pacific Plate (Schwartz & Rokosky 2007; Peng & Gomberg 2010). These include the Cascadia subduction zone (Rogers & Dragert 2003), the San Andreas Fault in central California (Nadeau & Dolenc 2005), the subduction zones in Mexico (Payero *et al.* 2008), Alaska (Peterson & Christensen 2009) and Costa Rica (Brown *et al.* 2009; Outerbridge *et al.* 2010). Tremors are often accompanied by slow-slip events observed from geodetic measurements (Rogers & Dragert 2003; Obara & Hirose 2006). Because tremors generally occur in the lower crust below the locked seismogenic zone, a systematic study of tremors and slow-slip events could help to better understand deep fault slips in the lower crust (Rubinstein *et al.* 2010), and their relationship to the occurrence of large earthquakes (Shelly 2009, 2010).

Recent studies have shown that tremor can be instantaneously triggered by passing surface waves of regional (epicentral distance between 100 and 1200 km) (Guilhem *et al.* 2010) and teleseismic earthquakes (Miyazawa & Mori 2005; Miyazawa & Mori 2006; Rubinstein *et al.* 2007; Gomberg *et al.* 2008; Miyazawa & Brodsky 2008; Miyazawa *et al.* 2008; Peng & Chao 2008; Peng *et al.* 2008; Ghosh *et al.* 2009; Peng *et al.* 2009; Rubinstein *et al.* 2009; Gomberg 2010; Peng *et al.* 2010a; Fry *et al.* 2011; Shelly *et al.* 2011). Triggered tremors are mostly found at places where

'ambient tremors' (i.e. not associated with teleseismic earthquakes) are identified, and their spectra shapes are similar (Rubinstein *et al.* 2007; Peng *et al.* 2008). In addition, at least portions of triggered tremor consists of many low-frequency earthquakes (LFEs) (Peng *et al.* 2010a; Tang *et al.* 2010; Shelly *et al.* 2011), suggesting that triggered and ambient tremors are generated by similar failure processes but with different loading condition. That is, triggered tremor could be considered as a special case of ambient tremor driven by the dynamic stresses from the surface waves (Gomberg 2010). Because triggered tremor generally has higher signal-to-noise ratio (SNR) than ambient tremor, and mostly occurs during the large-amplitude surface waves, it is relatively easy to search for triggered tremor in wide regions (e.g. Gomberg *et al.* 2008), hence providing a useful tool to identify regions with ambient tremors and slow-slip events (Gomberg 2010).

Although triggered tremor has been observed in many regions, several fundamental questions remain unclear. First, the underlying physical mechanisms of triggered tremor generation are still in debate. Earlier studies have suggested that triggered tremor reflects fluid flow due to changes in dilatational stresses during large-amplitude Rayleigh waves (Miyazawa & Mori 2005; Miyazawa & Mori 2006; Miyazawa & Brodsky 2008; Miyazawa *et al.* 2008). Recent studies have invoked simple Coulomb failure criteria (Hill 2008; Hill 2010) to explain the correlation of triggered tremor with both Love and Rayleigh waves (e.g. Rubinstein *et al.* 2007; Peng & Chao 2008; Peng *et al.* 2008; Peng *et al.* 2009; Rubinstein *et al.* 2009; Fry *et al.* 2011). In addition, the necessary conditions (both ambient environments and incoming surface waves) to favour triggered tremor generation are still unclear. The amplitude of passing surface waves appears to be an important factor in controlling triggered tremors based on the systematic surveys in Parkfield (Peng *et al.* 2009) and Cascadia (Rubinstein *et al.* 2009). Other factors, such as frequency (Guilhem *et al.* 2010) and incidence angle (Hill 2010) of surface waves are also possible controlling parameters for triggering tremor. Rubinstein *et al.* (2009) and Gomberg (2010) also suggested that when a fault is close to or undergoing failure, it is more likely to generate triggered tremor. Finally, triggered and ambient tremors occur in certain isolated regions along major plate boundaries (Beroza & Ide 2009; Peng & Gomberg 2010; Rubinstein *et al.* 2010; Beroza & Ide 2011). Although many studies have shown that elevated fluid pressures may favour tremor generation, it is still not clear what is the most important condition that control tremor occurrence.

To further investigate the necessary conditions and underlying mechanisms for triggered tremor, we conduct a systematic search of tremor in Taiwan triggered by large teleseismic earthquakes (Fig. 1). This study is an extension of our previous work on tremor triggered by the 2001 M_w7.8 Kunlun earthquake (Peng & Chao 2008), and LFEs triggered by the 2005 M_w8.6 Nias earthquake (Tang *et al.* 2010). In this study, we examine the passing surface waves from 45 teleseismic earthquakes between 1998 and 2009 with $M_w \geq 7.5$, and find a total of nine events that have triggered tremor in Taiwan. We present the results for these cases, and then discuss possible triggering mechanisms and necessary conditions for tremor generation.

2 TECTONIC SETTING AND PREVIOUS STUDIES OF TREMOR AND SLOW-SLIP EVENTS IN TAIWAN

Taiwan is a seismically active island located at the western portion of the circum-Pacific seismic belt. The high level of seismicity around Taiwan is mostly associated with two tectonic activities: the subduction of the Eurasian Plate eastwards beneath the Philippine Sea Plate on the southern side of the island, and the subduction of the Philippine Sea Plate northwards beneath the Eurasian Plate on the eastern side along the Ryukyu Trench (Shin & Teng 2001; Wu *et al.* 2007). In between, the Luzon Arc collides with the Chinese continental margin with a convergence rate of 7–8 cm yr^{-1} (Yu *et al.* 1997). The island itself can be divided into two major tectonic provinces, separated by the 160-km-long NNE-striking Longitudinal Valley Fault (LVF). The eastern side contains the Coastal Ranges and several volcanic islands. The western side can be further divided into several NNE–SSW trending structural belts: the Coastal Plain, Western Foothills, the Hsueshan Ranges and the Central Range (CR).

Several recent studies have focused on triggered tremors (Peng & Chao 2008; Velasco *et al.* 2009; Tang *et al.* 2010; Yeh 2011) and slow-slip events (Liu *et al.* 2009) in Taiwan. Peng and Chao (2008) first identified tremor beneath the southern CR triggered by the surface waves of the 2001 M_w7.8 Kunlun earthquake. The tremor occurs when the Love-wave displacement propagated to the southwest direction (parallel to the CR). They suggested that the tremor was generated by the shear slip on the weak detachment fault beneath the CR. Following the work of Guilhem *et al.* (2010) that searched for tremor triggered by regional earthquakes, Yeh (2011) conducted a systematic search of tremor along the CR triggered by 70 regional earthquakes around Taiwan with magnitude from 6.0 to 7.5 and epicentral distance between 100 and 2000 km, and did not find any positive case. One possible reason is that only recordings from surface stations were used in that study, and hence the SNR might be low in the examined frequency range of 2–8 Hz. Recently, Tang *et al*. (2010) used a matched filter technique to identify *P*- and *S*-waves of 41 LFEs within the tremor bursts triggered by the 2005 M_w8.6 Nias earthquake. They detected 1–2 LFEs in each tremor burst, and suggested that the triggered tremors consist of many LFEs, similar to ambient tremor (Shelly *et al.* 2007). Based on the LFE locations (yellow stars on Fig. 1), they proposed that those triggered LFEs (tremors) occurred on the deep extension of the high-angle thrust Chaochou-Lishan Fault (CLF) and near a region with modestly high V_p/V_s ratios (1.75–1.85). Velasco *et al*. (2009) studied the tremor triggering mechanism by modelling the triggering preference of surface waves based on the Coulomb failure criteria. They found that the Love wave produces the largest dynamic stress and triggers tremor when it propagates in the direction perpendicular to the strike of CR, while Rayleigh wave generates larger dynamic stress and triggers tremor when it propagates parallel to the strike of the CR. Moreover, Liu *et al*. (2009) reported slow earthquakes recorded by borehole strainmeter in eastern Taiwan near the LVF. These events generally last for a few hours to a day and half of them are triggered by typhoons.

3 DATA AND ANALYSIS PROCEDURE

The seismic data used in this study come from three major seismic networks in Taiwan: (1) the Broadband Array in Taiwan for Seismology (BATS) operated by the Institute of Earth Sciences (IES), Academia Sinica, (2) the short-period Central Weather Bureau Seismic Network (CWBSN) operated by the Taiwan Central Weather Bureau (CWB) and (3) the CWB Broadband Seismic Network (CWBBB) (Shin & Teng 2001). An additional temporary deployment, the TAiwan Integrated GEodynamics Research (TAIGER) (http://taiger.binghamton.edu/) was used for the 13

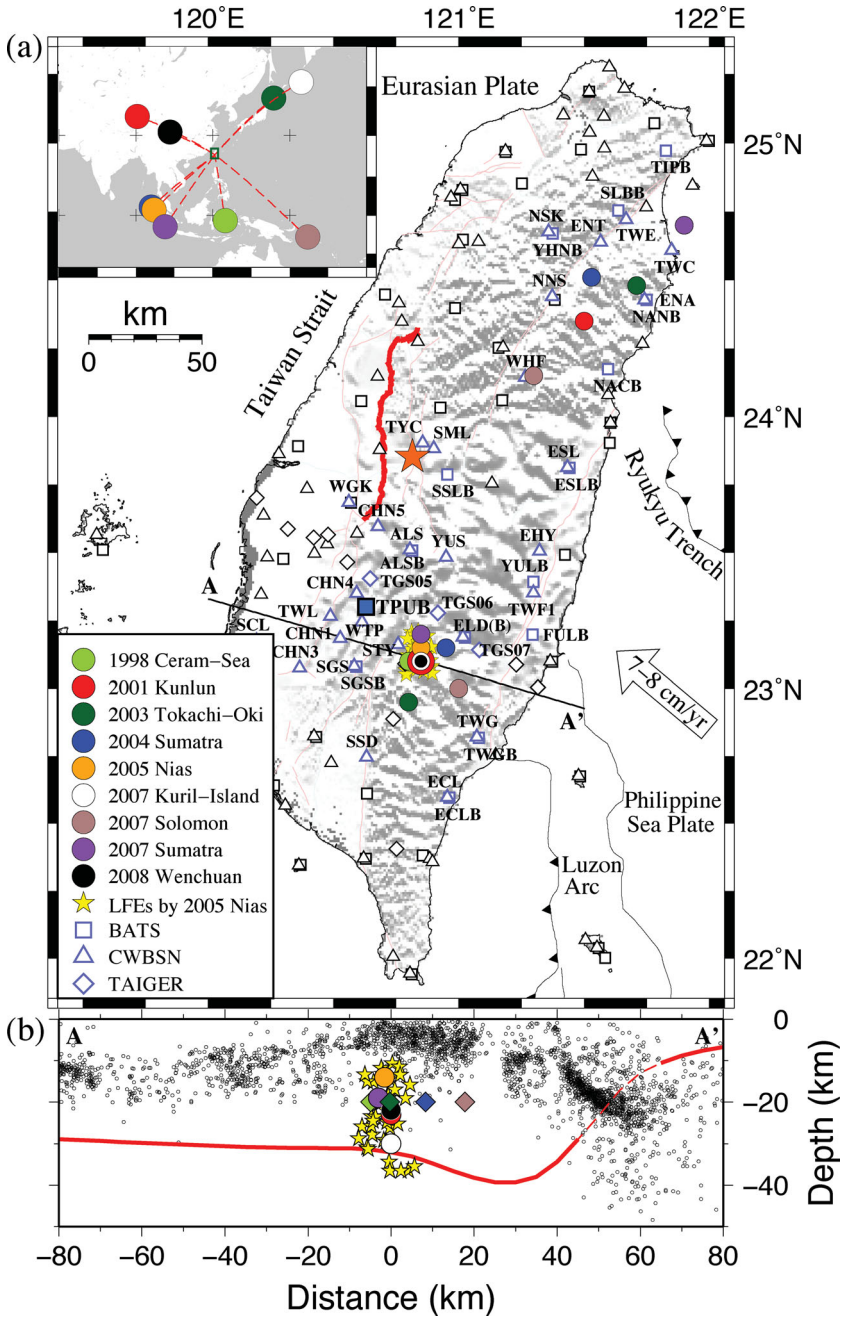

Figure 1. (a) The study area around the Central Range (CR) in Taiwan. The circles with different colours correspond to the locations of 14 tremors triggered by nine teleseismic earthquakes. The yellow stars mark the 41 low-frequency earthquakes (LFEs) (Tang *et al.* 2010) triggered by the 2005 Nias earthquake. Seismic stations of BATS, CWBSN and TAIGER are marked by square, triangle and diamond symbols, respectively. The stations plotted in light blue colours are used in this study. The broad-band station TPUB is shown by the blue square. The hypocentre and fault trace of the 1999 M_w7.6 Chi-Chi earthquake are marked by the orange star and red bold line. The inset shows the epicentral locations of the nine triggering main shocks. (b) A cross-section view along A–A′ normal to the strike of the southern CR. Triggered tremors and LFEs are marked by circles and stars, respectively. The diamond symbols mark the tremor locations that are not well constrained and set to be at 20 km. The black dots represent earthquakes with magnitudes greater than 3.0 within 20 km along A–A′ between 1991 and 2006 from the CWBSN catalogue. The red line marks the Moho depth calculated by the receiver functions (Tang *et al.* 2011).

January 2007 M_w8.1 Kuril-Island earthquake. We selected large teleseismic earthquakes from 1998 January 01 to 2009 December 31 listed in the Advanced National Seismic System (ANSS, http://www.ncedc.org/anss/) earthquake catalogue. A total of 45 earthquakes (Fig. 2a) with magnitudes $M_w \geq 7.5$, depths ≤ 100 km and epicentral distances ≥ 1000 km to the BATS station TPUB (Fig. 1a) were selected for further examination (Table S1). These criteria are based on the empirical values used by recent studies of tremor triggered by teleseismic earthquakes in other regions (Peng *et al.* 2009; Rubinstein *et al.* 2009).

The analysis procedure generally follows that of Peng & Chao (2008) and Peng *et al*. (2009) and is briefly described here. We first shifted the reference time of three-component (north, east and vertical) seismograms to the origin time of the teleseismic event, removed mean and instrument response, cut seismograms into the lengths of 1000 s before and 9000 s after the origin time and applied

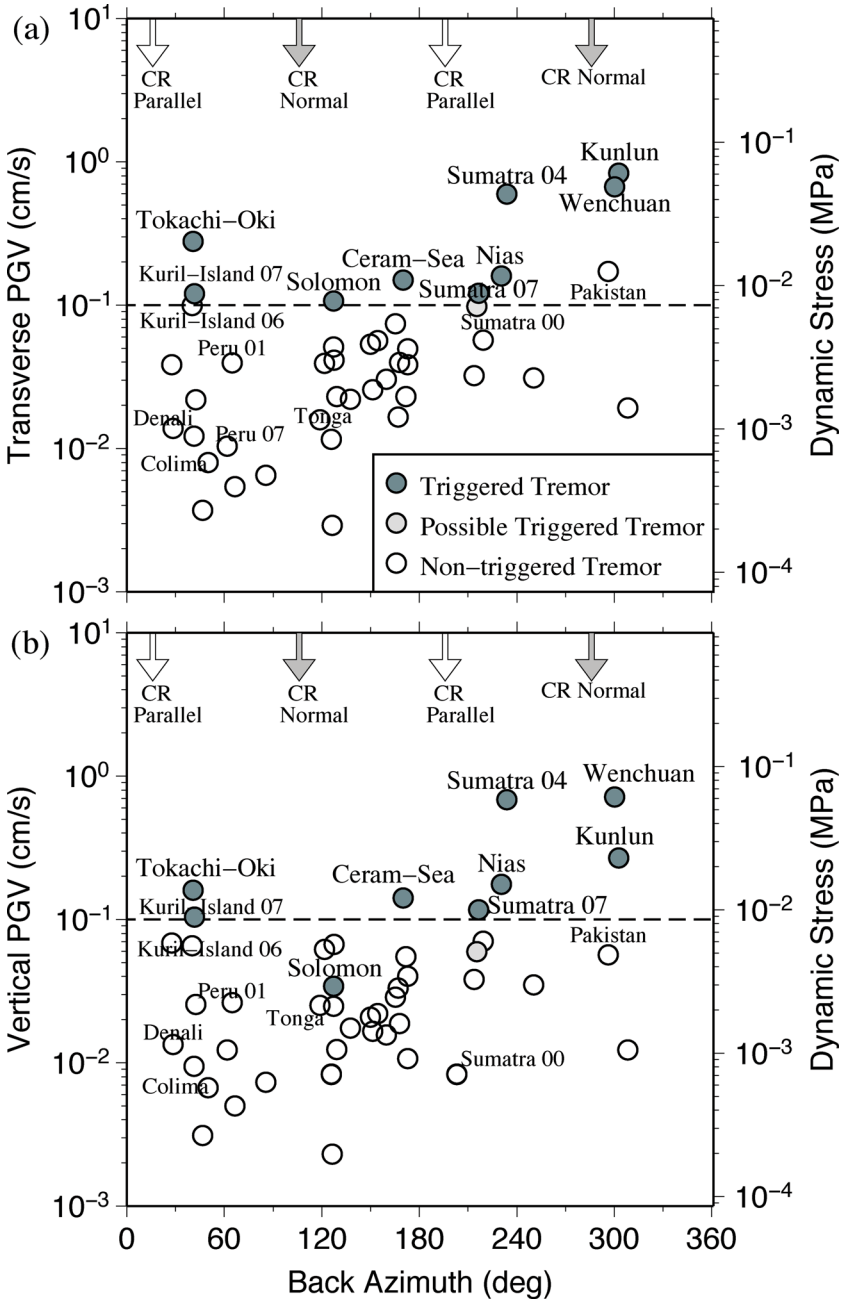

Figure 2. The peak ground velocity (left vertical axis) and the corresponding dynamic stress (right vertical axis) versus the backazimuth in transverse (a) and vertical (b) components at station TPUB for all 45 teleseismic earthquake with $M_w \geq 7.5$ between 1998 and 2009. The dashed line marks the apparent tremor-triggering threshold of 7–8 KPa. The solid white and grey arrows mark the directions parallel and normal to the strike of the Central Range (CR, N16°E). The detailed earthquake information is listed in Table S1.

a 2–8 Hz bandpass filter. Next, we compared the bandpass-filtered seismograms with the broad-band recordings to visually identify triggered tremor during the passage of surface waves. Only the seismic data recorded by the BATS were used in this step because this is the only network with continuous recording throughout the entire time period. We identified triggered tremor as bursts of high-frequency, non-impulsive and long-duration seismic signals that are coherent among many nearby stations, and in phase with the passing surface waves (Peng *et al.* 2009). If the comparison with BATS stations showed potential triggered tremor signals, we examined the CWB broad-band and short-period data for further evidence of triggered tremor. Only the signals recorded by at least five surrounding stations within 100 km of the potential tremor source with clear moveout (i.e. later arrivals with increasing distances) are classified as positive triggering cases and used in the following analysis.

Next, we used the standard envelope cross-correlation techniques (Peng & Chao 2008; Peng *et al.* 2009) to obtain the tremor location by minimizing the rms residual between the theoretical travel-time difference among station pairs and those observed from cross-correlations of bandpass-filtered envelope functions. Based on the tremor moveout and our previous studies, we divided the seismic data into two groups, one around the southern CR, and the other one near the northern CR (Fig. 1a). We assumed that multiple tremor episodes triggered by the same teleseismic earthquake come from

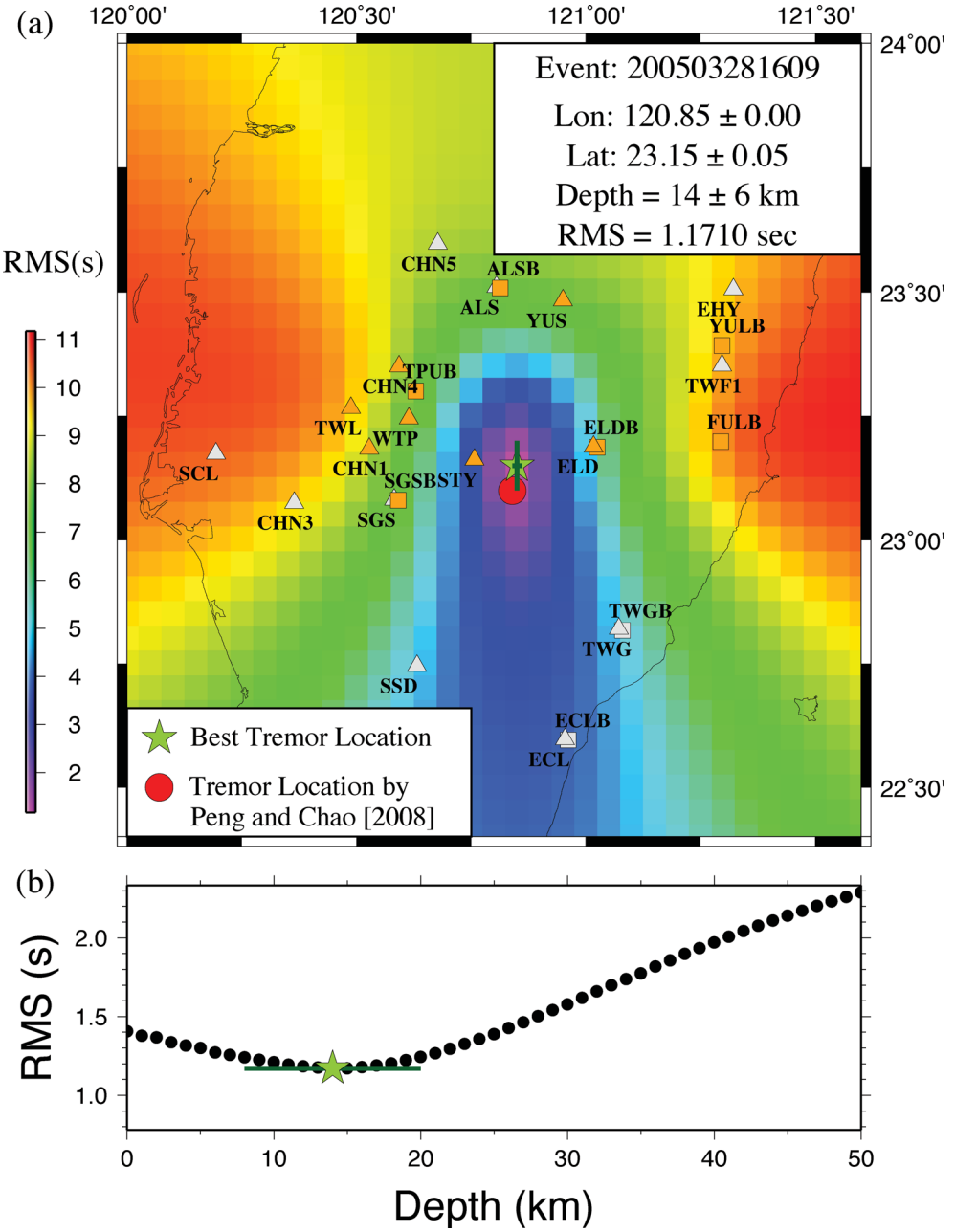

Figure 3. (a) An example of tremor location triggered by the 2005 Nias earthquake. The background colour marks the rms residual between the observed and predicted traveltime differences, and the best tremor location that corresponds to the minimum rms is marked by the green star. The red circle marks the hypocentre of tremor triggered by the 2001 Kunlun earthquake (Peng & Chao 2008). The orange symbols mark the stations that are used to locate tremor. Other notations are the same as in Fig. 1. (b) The rms versus depth profile at the hypocentre of the best tremor location. The green star marks the best fitting depth and the horizontal line shows the 68 per cent confidence level.

the same location, either in the southern or northern CR. Although tremor (or LFEs) triggered by the same triggering event could come from slightly different sources (Fig. 1b, Tang *et al.* 2010), in general those LFEs triggered by the 2005 Nias earthquake are close to the location (Fig. 1a) identified by the envelope cross-correlation techniques. Hence in this study we only calculated an average location in southern or northern CR for each triggering event. We used an updated 1-D velocity model (Tang *et al.* 2010) to compute the *S*-wave arrival times for the tremor from south. This 1-D velocity model (Table S2a) is averaged from the 3-D velocity model (Wu *et al.* 2007) around the southern tremor source region. For the tremor locations in north, we used a slightly different 1-D velocity model (Table S2b) computed from the 3-D velocity model (Wu *et al.* 2007) in that region. Finally, we computed the rms values using a 1 km grid from 0 to 50 km in depth and within 1° of the epicentral distance from the stations ELDB and ENT for the tremor in southern and northern CR, respectively. The best tremor location is obtained from the smallest rms and the location errors were calculated from the chi-square distribution within the 68 per cent confidence limit (Shearer 1999). An example of the best-fitting tremor locations triggered by the 2005 Nias earthquake is shown in Fig. 3.

Fig. 1(a) shows the tremor locations in southern and northern CR. The tremors in the southern CR are clustered in a restricted region, while the tremor locations in the northern CR are more scattered.

The horizontal and vertical uncertainties in tremor locations are on the order of 10 km (see Table S3 for detailed error estimation), which is typical for those locations obtained from the tremor envelope cross-correlation techniques (Obara 2002; Rubinstein *et al.* 2010). The depths of tremors were general located between 15 and 25 km (Fig. 1b). For some events the depths were not well constrained because the rms value decreasing or increasing monotonically with depth, we used an average value of 20 km in depth for those events (diamond symbols in Fig. 1b).

4 TREMORS TRIGGERED BY TELESEISMIC EARTHQUAKES

Among all 45 teleseismic earthquakes (Fig. 2), we identified nine earthquakes (Table S3) that triggered nine and five tremor sources in the southern and northern CR (Fig. 1a), respectively. These earthquakes include the (1) 1998 November 29 M_w 7.7 Ceram Sea, (2) 2001 November 14 M_w7.8 Kunlun, (3) 2003 September 25 M_w8.3 Tokachi-Oki, (4) 2004 December 26 M_w9.2 Sumatra, (5) 2005 March 28 M_w8.6 Nias, (6) 2007 January 13 M_w8.1 Kuril-Island, (7) 2007 April 1 M_w8.1 Solomon, (8) 2007 September 12 M_w8.4 Sumatra and (9) 2008 May 12 M_w7.9 Wenchuan earthquakes (Figs 4–12). In addition, the 2000 June 4 M_w7.9 Sumatra earthquake (Fig. 13) is considered as a possible triggering event due to lack of enough recording stations.

To better quantify whether Love or Rayleigh waves trigger tremor in the southern CR, we used the following three criteria to measure the effects of surface waves on tremor activity. First, we checked whether the tremor activity is initiated by the Love or the Rayleigh waves. If tremor starts in the first few cycles of the Love waves, then it is considered as a possible case of Love wave triggering (e.g. Fig. 4). On the other hand, if tremor did not start until the arrivals of the long-period Rayleigh waves, then it is likely that Rayleigh wave plays a more important role in triggering tremor (e.g. Fig. 7). Because Rayleigh wave introduces volumetric changes (Miyazawa & Brodsky 2008), we evaluated Rayleigh-wave triggering in upward vertical surface displacement (BHZ in Figs 4–12b) to represent the positive dilatational (volumetric) stress changes at depth (Peng *et al.* 2009). The Love-wave amplitude decreases with depth and such displacement gradient would cause horizontal shear that is either parallel or perpendicular to the wave propagation direction (Hill 2008). Because most of the tremor-triggering events have incidence angles that are either parallel or perpendicular to the strike of the CR, we used the peak of the Love-wave displacement in the transverse component (BHT seismogram in Figs 4–12b) as a proxy to represent shear stresses at depth where tremor occurred (Peng & Chao 2008). We computed the *S*-wave traveltime at the station with best tremor signals and shifted the trace back to the tremor source region. Similarly, we time shifted the surface waves traces based on phase velocities of 4.1 km s^{-1} and 3.5 km s^{-1} for the Love and Rayleigh waves, respectively. Finally, we compared the peaks of the tremor bursts on the time-shifted 2–8 Hz bandpass-filtered envelope functions, with the time-shifted surface wave peaks. Secondly, we compared the peak displacement amplitudes ratio of Rayleigh and Love waves (R/L) and used it as a proxy for the strength of the associated dynamic stresses. When the R/L value is greater than 1, it means that the Rayleigh-wave amplitude is larger than the Love-wave amplitude, and vice versa. We noted that the peak amplitudes are measured on the surface, and they decay differently with depth. Nevertheless, their amplitude ratios provide a first-order approximation of the induced stress perturbations. Thirdly, we computed the correlation coefficient (CC) between time-shifted tremor envelope functions and Love (CC-Lo) and Rayleigh (CC-Ra) waves. Ideally, if tremor is mostly triggered by certain types of surface waves, then we would expect to see relatively high positive CC values between surface waves and tremor envelopes. Hence, we used the CC value as a measure of their correlations.

In the following subsections, we describe the observed triggered tremors and quantify their relationships to the surface waves for all nine triggering earthquakes. Figs 4–12 are presented in the order from the maximum to minimum transverse peak ground velocity (PGV) recorded at the BATS station TPUB (Fig. 2a). In each event, we considered it as a Love- or Rayleigh-wave triggering case if at least two of the three aforementioned criteria are met.

4.1 The 2001 November 14 M_w7.8 Kunlun earthquake

The 2001 November 14 M_w7.8 Kunlun earthquake generated the largest transverse PGV (Fig. 2a) at the station TPUB, and has triggered microearthquakes near Beijing (Wu *et al.* 2011), and tremor in central California (Peng *et al.* 2009). This event also triggered clear tremor beneath the southern CR in Taiwan (Peng & Chao 2008), and the results are briefly summarized here. The 2–8 Hz bandpass-filtered seismograms show clear triggered tremor (Fig. 4a) from at least two tremor sources, one near the southern CR where the majority of the triggered tremor (Fig. 1a) and LFEs (Tang *et al.* 2010) are located, and another is located in the northern portion of the CR (Fig. 1a). Additional tremor bursts appeared later with the long-duration surface waves until 1350 s. Tremor sources appear to be initiated by the Love wave (Fig. 4b) and the amplitude ratio is less than 1 (R/L = 0.21). Hence this event is considered as Love-wave triggering (Peng & Chao 2008) even though the tremor bursts are correlated better with the small-amplitude Rayleigh wave (CC-Ra = 0.36 and CC-Lo = 0.03).

4.2 The 2008 May 12 M_w7.9 Wenchuan earthquake

The 2008 May 12 M_w7.9 Wenchuan earthquake generated the second largest PGV (Fig. 2a) in transverse components at the station TPUB, and has the closest epicentral distance of about 1900 km to TPUB among all 45 teleseismic earthquakes. This event also triggered widespread microearthquakes in continental China (Jiang *et al.* 2010; Peng *et al.* 2010b), tremor in southwest Japan (Miyazawa *et al.* 2008), Cascadia (Gomberg 2010) and central California (Peng *et al.* 2009). Interestingly, this event only triggered tremor signals (Fig. 5a) that are barely above the background noise levels during the main shock coda between 600 s and 850 s near the southern CR in Taiwan. After shifting both the tremor and the surface waves back to the tremor source region, we find that tremor did not occur during the first few cycles of Love wave starting at ∼600 s (Fig. 5b), but are modulated by the following Rayleigh waves (∼680 s). Also the tremor and Rayleigh wave is correlated better (CC-Ra = 0.50 and CC-Lo = 0.20), thus we classified this event is triggered by Rayleigh waves.

4.3 The 2004 December 26 M_w9.0 2004 Sumatra earthquake

The 2004 December 26 M_w9.0 Sumatra earthquake has the largest magnitude among all the analysed events and generated the third largest transverse PGV (Fig. 2a) among all nine triggering events in Taiwan. This event also triggered tremor in central California (Ghosh *et al.* 2009; Peng *et al.* 2009), Cascadia (Rubinstein

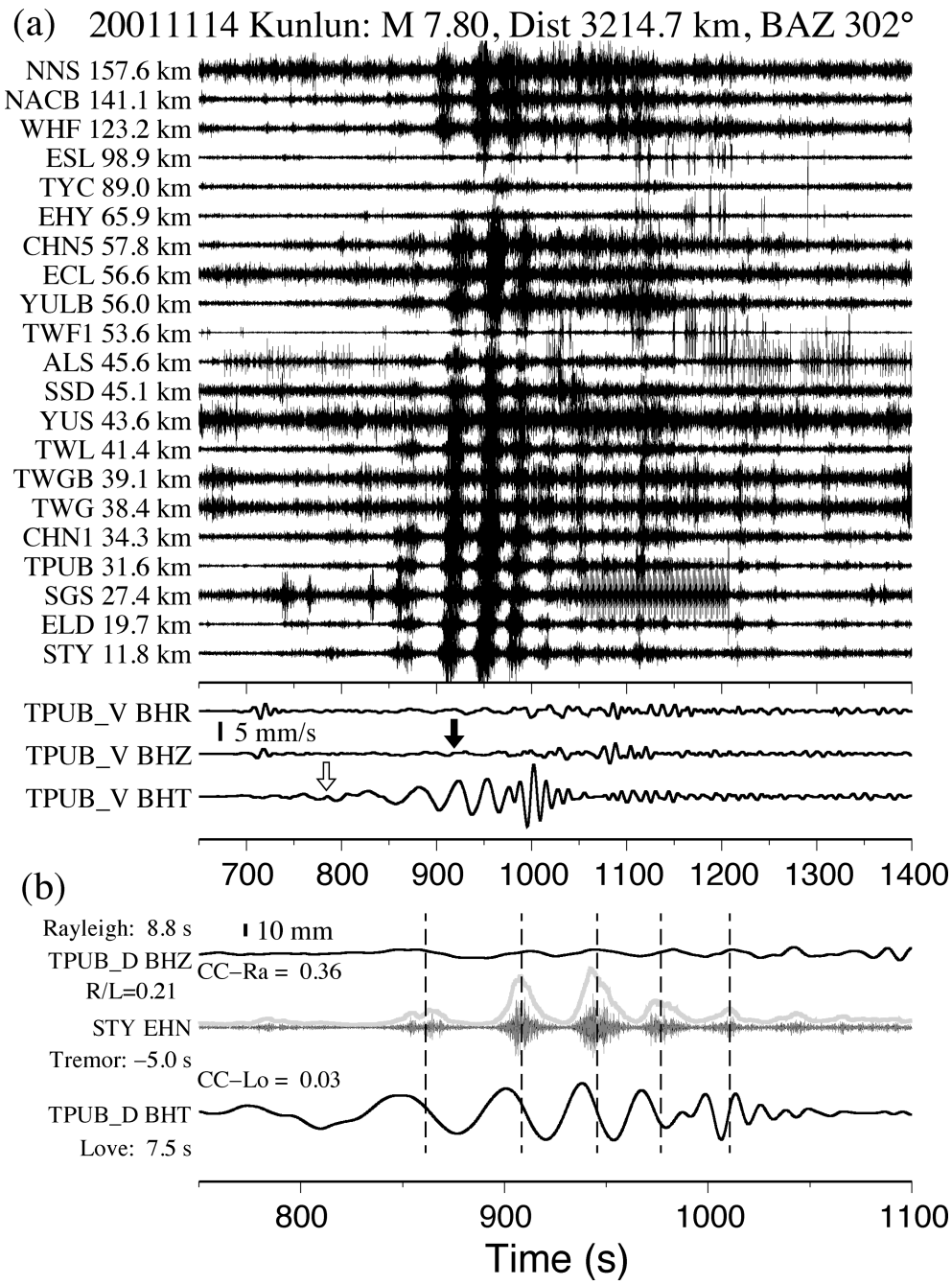

Figure 4. Tremor triggered by the 2001 M_w7.8 Kunlun earthquake. (a) The 2–8 Hz bandpass-filtered seismograms in the north (N) component showing the moveout of tremor from two source regions. The seismograms are plotted according to the best tremor location in the southern CR. The hypocentral distance between each station and tremor source is shown next to the station name on the left-hand side of each trace. The occurrence date (year/month/day) of the main shock, its magnitude (M) and the epicentre distance (Dist) and backazimuth (BAZ) relative to the broad-band station TPUB are shown on the top. The lower panel of (a) shows the radial (R), vertical (Z) and transverse (T) component velocity (V) seismograms recorded at station TPUB. The thick vertical bars mark the amplitude scale of surface waves. The zero time corresponds to the origin time of the main shock. The open and black vertical arrows indicate the predicted arrivals of the Love and Rayleigh waves with the apparent velocity of 4.1 and 3.5 km s^{-1}, respectively. (b) A detailed comparison between the displacement (D) seismograms in Z component for Rayleigh wave and T component for Love wave at TPUB and 2–8 Hz bandpass-filtered N-component seismogram at a CWB station STY. Each seismogram has been time-shifted back to the tremor occurrence time to reflect the relationship between the surface waves and tremor at the source region. The adjusted times for Rayleigh waves, Love waves and tremor are marked next to the station names. The maximum amplitude ratio of Rayleigh/Love (R/L) waves is measured during the tremor occurrence time. The vertical dotted lines mark the peaks of tremor envelope functions. The correlation coefficient (CC) between time-shifted tremor envelope functions and Love (CC-Lo) and Rayleigh (CC-Ra) waves are shown by each seismogram. The time windows used to compute the CC values (Table S3) generally started around the predicted arrivals and centred around the peaks of the Love and Rayleigh waves.

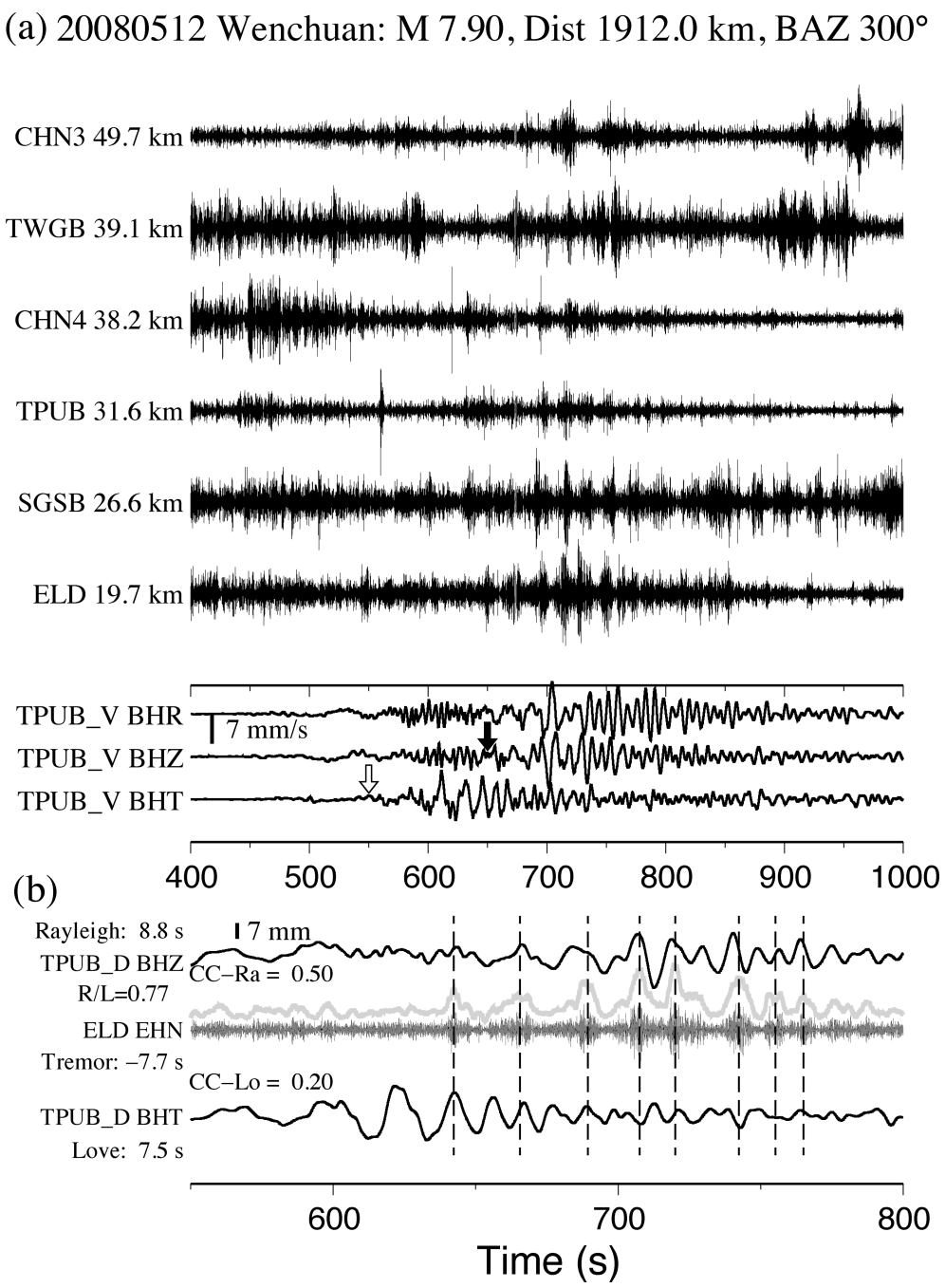

Figure 5. Tremor triggered by the 2008 M_w7.9 Wenchuan earthquake. (a) The 2–8 Hz bandpass-filtered N-component seismograms showing moveout of triggered tremor during the passing surface waves between 600 and 850 s. (b) A detailed comparison between the displacement seismograms at TPUB and bandpass-filtered seismogram at CWB station ELD. Other notations are the same as in Fig. 4.

et al. 2009) and southern Japan (Miyazawa & Mori 2006; Miyazawa & Brodsky 2008), and microearthquakes near Beijing, China (Wu *et al.* 2011) and Alaska (West *et al.* 2005). The 2004 Sumatra earthquake generated clear multiple tremor sources in both southern and northern CR in Taiwan (Fig. 6a). Some tremor bursts started to appear at 950 s and the large-amplitude tremor bursts occurred between 1150 s and 1450 s. Small tremor bursts appeared until 1600 s. The tremor bursts show better correlation with larger amplitude of Rayleigh waves (R/L = 1.28, CC-Ra = 0.23 and CC-Lo = –0.44, Fig. 6b). Hence, we consider this as a case of Rayleigh-wave triggering.

4.4 The 2003 September 25 M_w8.3 Tokachi-Oki earthquake

The 2003 September 25 M_w8.3 Tokachi-Oki earthquake in Japan has the fourth largest transverse PGV (Fig. 2a). This event triggered shallow microearthquakes near Beijing (Wu *et al.* 2011), tremor in southwest Japan (Miyazawa & Mori 2005; Miyazawa *et al.* 2008), central California (Peng *et al.* 2009) and multiple tremor sources in Taiwan (Fig. 7a). Tremors triggered by this event are shown between 750 and 1200 s (Fig. 7a). Due to lack of continuous CWBSN data during this time, we only used data from BATS and CWBBB networks to analyse this event. After shifting time back to the tremor

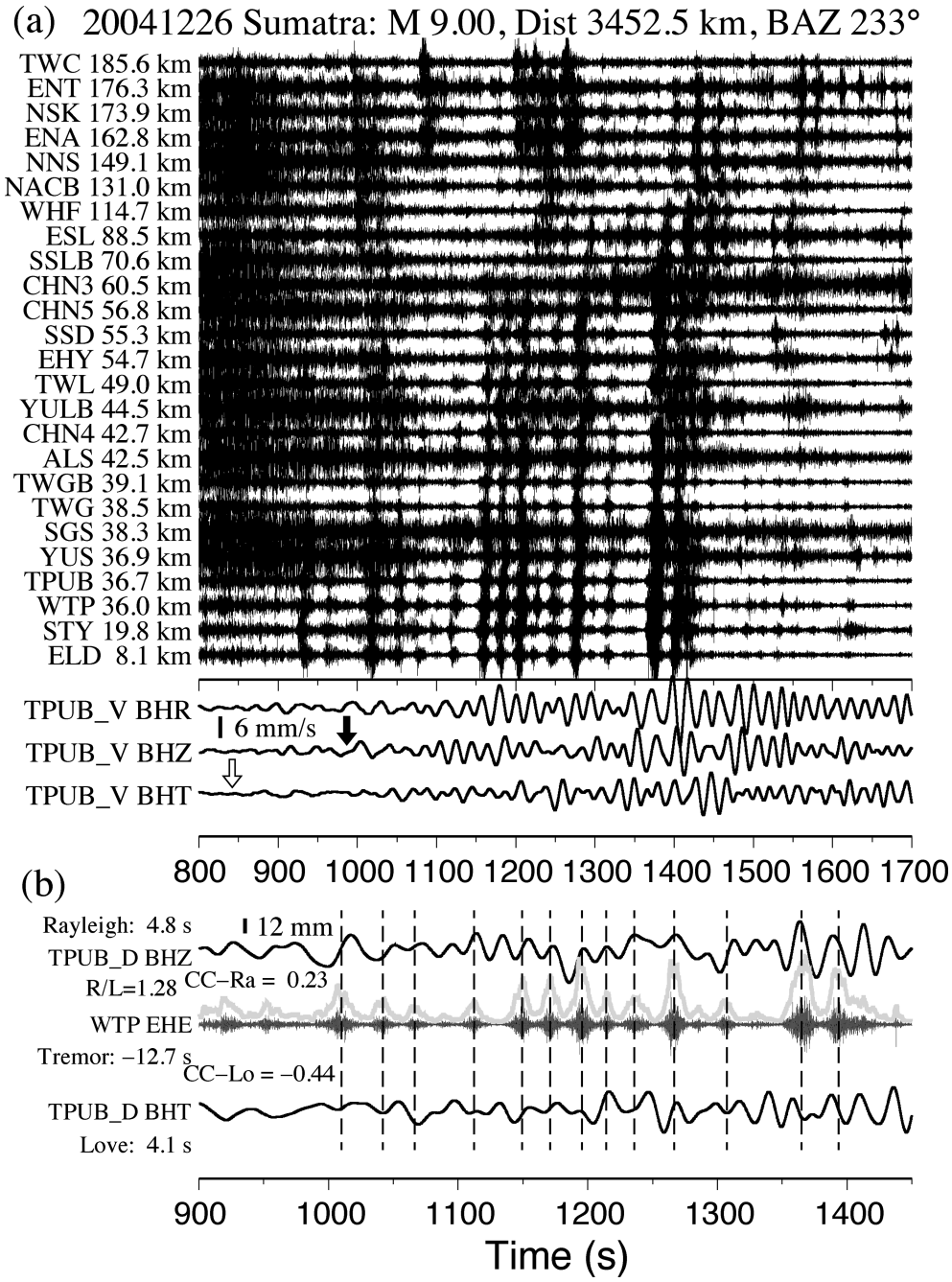

Figure 6. Tremor triggered by the 2004 M_w9.0 Sumatra earthquake. (a) The 2–8 Hz bandpass-filtered E-component seismograms showing moveout of tremor from multiple source regions. (b) A detailed comparison between the displacement seismograms at TPUB and bandpass-filtered seismogram at WTP. Other notations are the same as in Fig. 4.

source region, we found that the first tremor burst in the southern portion occurred at ∼780 s after the first arrival of Love waves (Fig. 7b). On the other hand, the tremor peaks corresponded well with the peaks of Rayleigh waves (Fig. 7b, CC-Ra = 0.39 and CC-Lo = –0.24), hence this event is considered as triggered by Rayleigh waves.

4.5 The 2005 March 28 M_w8.6 Nias earthquake

The 2005 March 28 M_w8.6 Nias earthquake in Sumatra, Indonesia has the second largest magnitude and has the fifth largest transverse PGV among all nine triggering earthquakes. This event generated a single tremor source in the southern CR. The clear tremor bursts were shown between 950 s and 1300 s (Fig. 8a), and the long-duration tremor bursts were continuously shown up until 2200 s. The large-amplitude signals recorded at around 1400 s, 1750 s and 2150 s possibly came from three local earthquakes (marked by vertical grey arrows in Fig. 8a) with M2.3 near Chiayi City (120.37°E, 23.53°N and 9 km in depth), M2.7 at about 40 km north of Hualien City (121.73°E, 24.25°N and 13 km in depth), and M2.2 at about 37 km north of Hualien City (121.72°E, 24.25°N and 12 km in depth), respectively. After adjusting the times of tremor and surface waves, the comparison indicates that the tremors were more

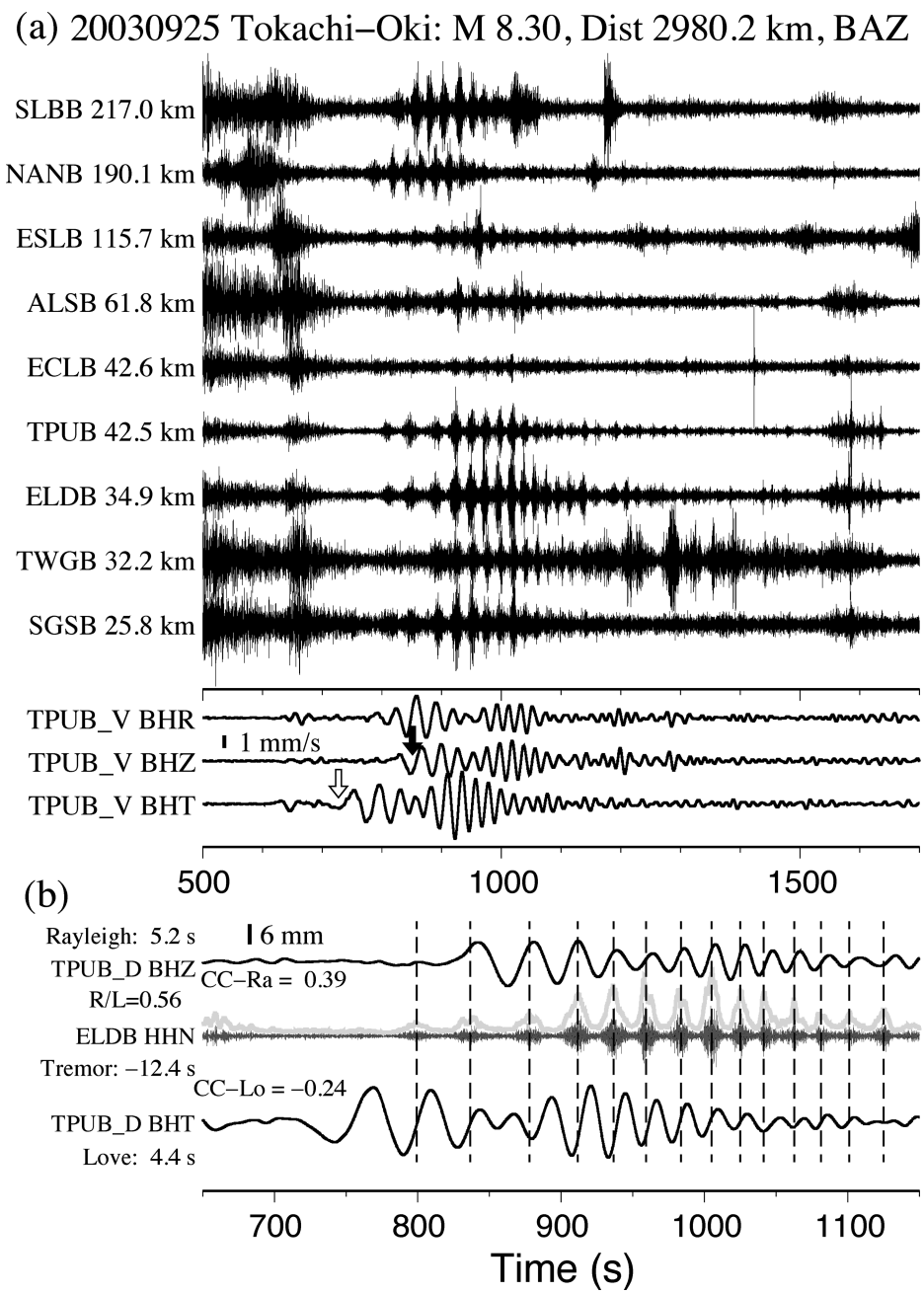

Figure 7. Tremor triggered by the 2003 M_w8.3 Tokachi-Oki earthquake. (a) The 2–8 Hz bandpass-filtered N-component seismograms showing moveout of tremor from multiple source regions. (b) A detailed comparison between the displacement seismograms at TPUB and bandpass-filtered seismogram at ELDB. Other notations are the same as in Fig. 4.

likely associated with Rayleigh waves (Fig. 8b, R/L = 2.53, CC-Ra = 0.48, and CC-Lo = 0.39). Again, we consider this as a Rayleigh wave triggering case.

4.6 The 1998 November 29 M_w7.7 Ceram Sea earthquake

The 1998 November 29 M_w7.7 Ceram Sea earthquake has the smallest magnitude among all the nine tremor triggering events and has the second closest epicentral distance of about 2800 km to TPUB. This event generated triggered tremors in the south of the CR shown between 850 and 1000 s (Fig. 9a). The tremor bursts were barely above the background noise level, and mostly occurred during the Rayleigh waves (Fig. 9b, R/L = 1.54, CC-Ra = 0.28 and CC-Lo = –0.07).

4.7 The 2007 September 12 M_w8.4 Sumatra earthquake

The 2007 September 12 M_w8.4 Sumatra earthquake has one of the smallest transverse PGV (Fig. 2a) and generated two clear tremor sources in both southern and northern CR (Fig. 1a). The clear tremor bursts from the southern CR occurred between 1000 s and 1900 s during the passing surface waves (Fig. 10a). Tremors around the northern CR occurred during 1100–1500 s and were recorded by three stations TIPB, ENT and NANB. Based on the comparison between surface waves and tremor bursts in Fig. 10(b), the tremor

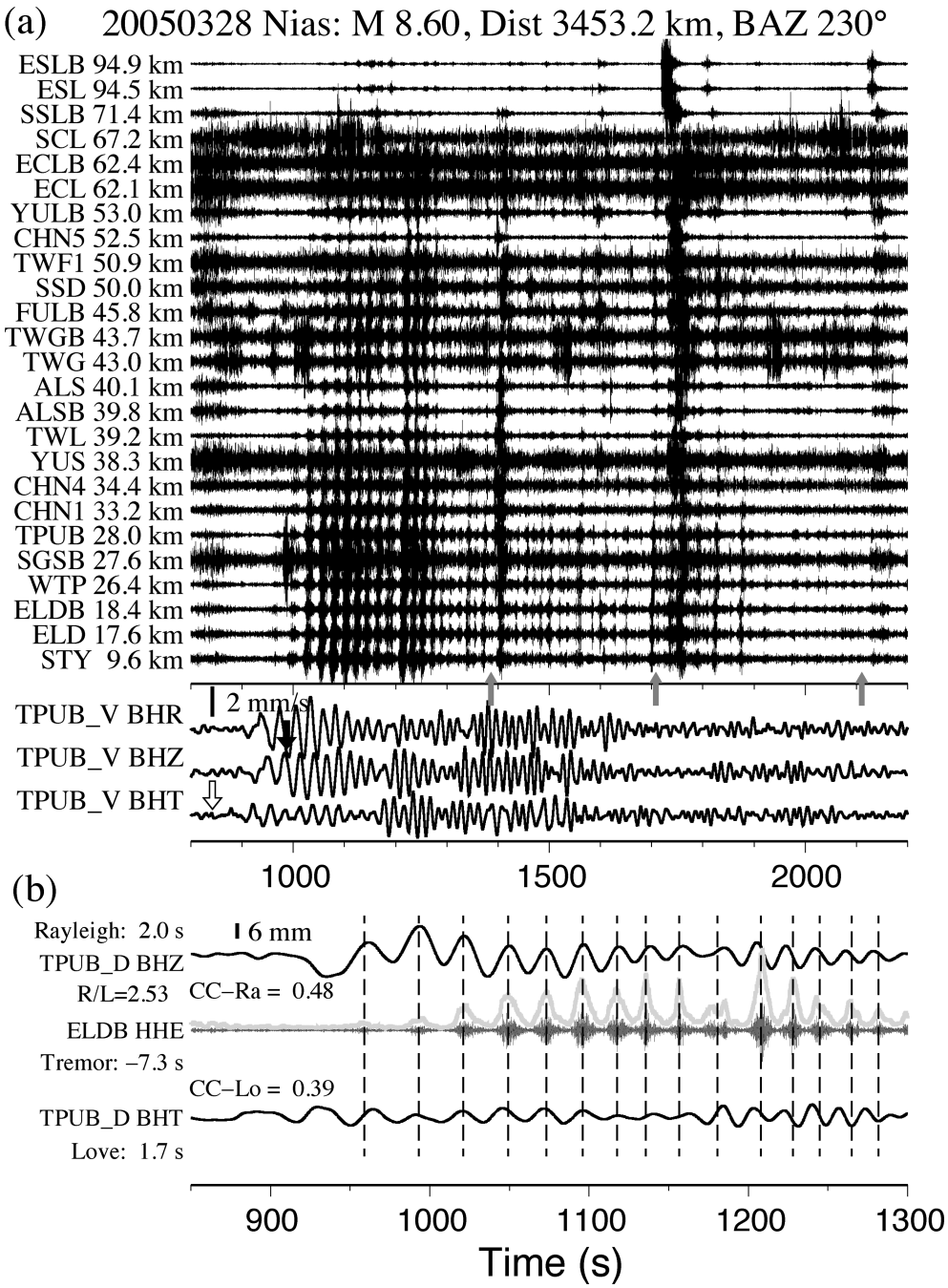

Figure 8. Tremor triggered by the 2005 M_w8.6 Nias earthquake. (a) The 2–8 Hz bandpass-filtered E-component seismograms showing moveout of tremor from the southern CR. The vertical grey arrows mark the origin times of local earthquakes from the CWB catalogue. (b) A detailed comparison between the displacement seismograms at TPUB and bandpass-filtered seismogram at ELDB. Other notations are the same as in Fig. 4.

sources from the south of the CR were mainly associated with the Rayleigh waves (R/L = 2.37, CC-Ra = 0.35 and CC-Lo = 0.04).

4.8 The 2007 January 13 M_w8.1 Kuril Island earthquake

The 2007 January 13 M_w8.1 Kuril Island earthquake in Japan has one of the smallest transverse PGV (Fig. 2a) among all nine triggering earthquakes. This earthquake and the previous M_w8.3 Kuril Island earthquake occurred on 2006 November 15, both triggered tremors in central California (Peng *et al.* 2009). In Taiwan, although the measured transverse PGVs for both events are very close (Fig. 2a), only the 2007 Kuril Island event shows clear triggered tremor signals in the southern CR. The tremor bursts started at 1100 s and continuously appeared until 2100 s (Fig. 11a). The impulsive signals recorded at around 2100 s came from a local earthquake (marked by vertical grey arrow in Fig. 11a) with M3.0 located at the Pacific Ocean around 90 km outside the Hualien City (122.47°E, 24.15°N and 45 km in depth). After adjusting the occurrence time of surface waves and tremors back to the tremor sources, we found that tremor started during the Rayleigh waves. In addition, the tremor bursts correlated better with Rayleigh wave (CC-Ra = 0.23 and CC-Lo = 0.11). Hence we also consider this is triggered by Rayleigh waves.

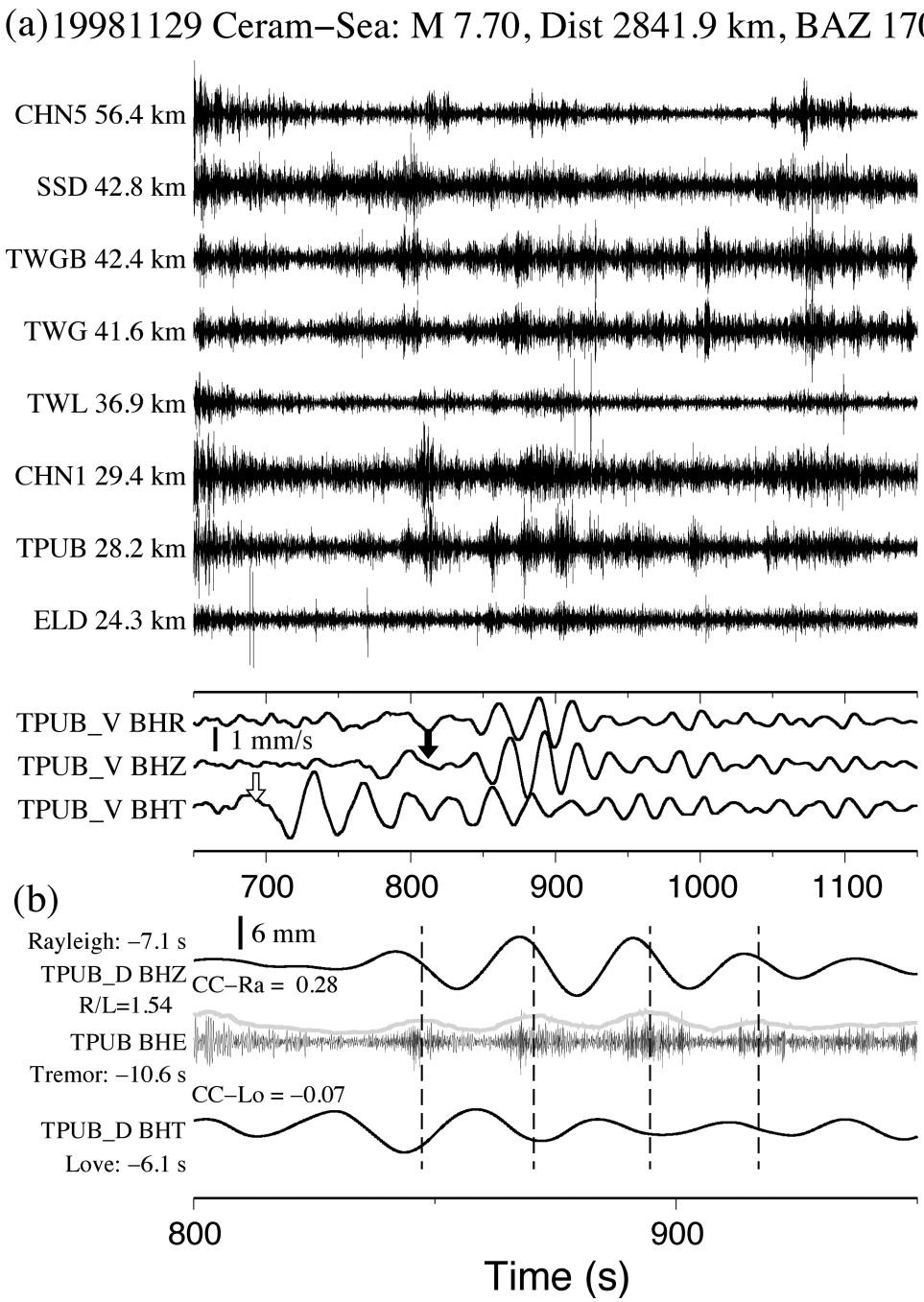

Figure 9. Tremor triggered by the 1998 M_w7.7 Ceram Sea earthquake. (a) The 2–8 Hz bandpass-filtered seismograms in the E-component showing the moveout of tremor from the southern CR. (b) A detailed comparison between the displacement seismograms and bandpass-filtered seismogram recorded at TPUB. Other notations are the same as in Fig. 4.

4.9 The 2007 April 1 M_w8.1 Solomon Islands earthquake

The 2007 April 1 M_w8.1 Solomon Islands earthquake has the least transverse and vertical PGV (∼0.1 cm s^{-1}) at TPUB (Fig. 2). This event also generated triggered tremors in the southwest Japan (Miyazawa *et al.* 2008). In Taiwan, this event triggered multiple tremor sources with low SNR between 1350 s and 1450 s (Fig. 12). The tremor source around the southern CR was located further to the southeast as compared with other tremor sources (Fig. 1). Another tremor source located in the north (Fig. 1a) was recorded at stations with epicentral distance greater than 100 km. After adjusting time back to the tremor source region in the southern CR, we found that the tremor bursts occurred far after the arrival of Love waves (at ∼1250 s). Also the tremor bursts correlate better with larger amplitude of Rayleigh waves (R/L = 1.89, CC-Ra = 0.23 and CC-Lo = 0.13), hence we considered this is triggered by Rayleigh waves.

4.10 The 2000 June 4 M_w7.9 Sumatra earthquake

The 2000 June 4 M_w7.9 Sumatra earthquake has one of the smallest transverse and vertical PGV by comparing with the other nine triggering events (Fig. 2). We found clear tremor bursts consistent with the cycles of Rayleigh waves between 1000 and 1400 s (Fig. 13)

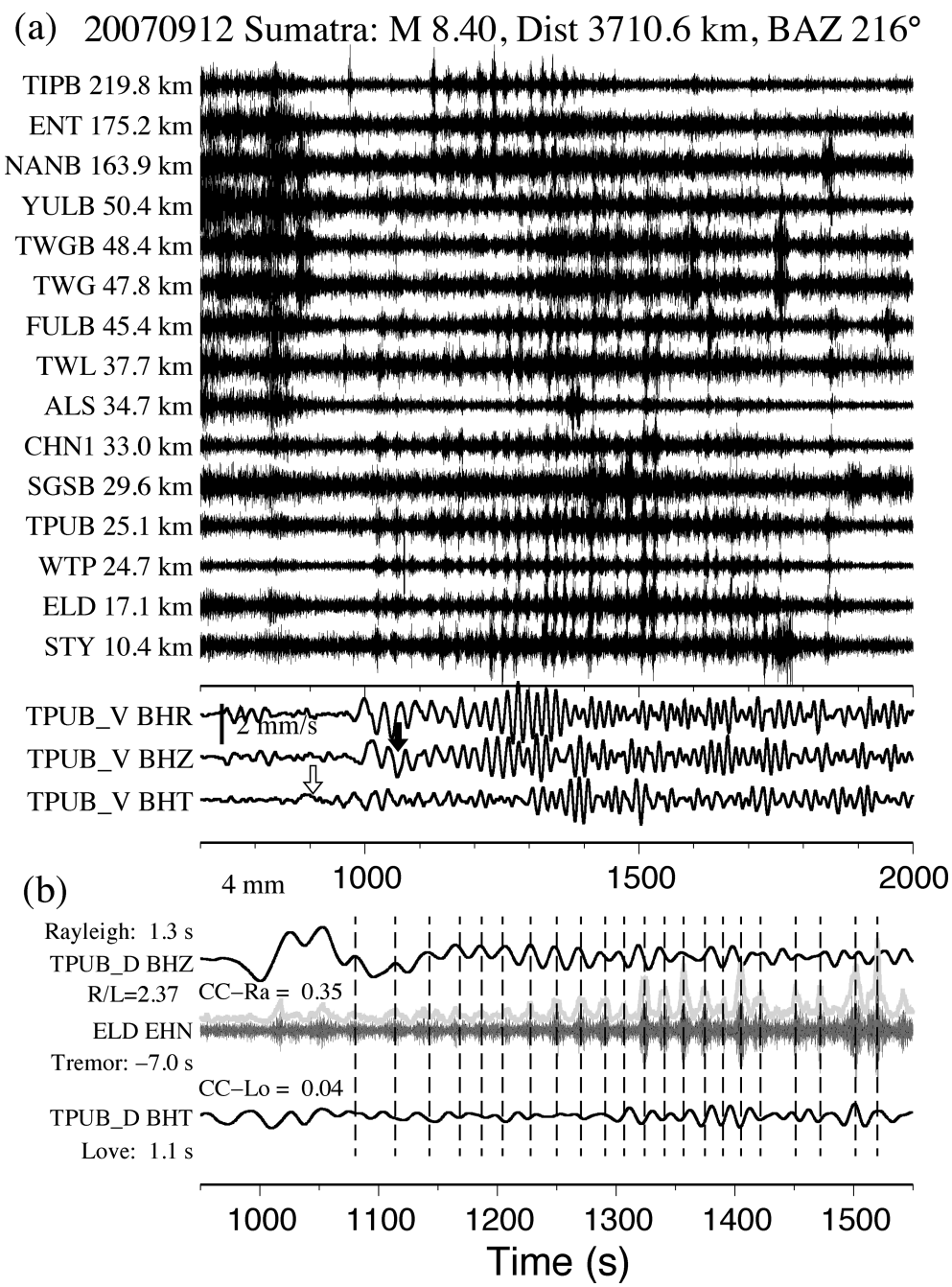

Figure 10. Tremor triggered by the 2007 M_w8.4 Sumatra earthquake. (a) The 2–8 Hz bandpass-filtered seismograms in the N-component showing the moveout of tremor from the multiple sources. (b) A detailed comparison between the displacement seismograms at TPUB and bandpass-filtered seismogram at ELD. Other notations are the same as in Fig. 4.

at TPUB station of BATS. However, due to the lack of continuous CWBSN data during this time to further confirm and locate the tremor, we considered this as a case of possible triggered tremor. The impulsive signal recorded at around 640 s came from a local earthquake with magnitude 2.8 located at the Pacific Ocean around 30 km southeast of the Yilan City (121.97°E, 24.38°N and 28 km in depth). The double peaks at around 900 s during the large-amplitude Love waves likely correspond to a regional earthquake (with $S-P$ time of ∼15 s) because no local earthquakes are listed in the CWB catalogue during this time period.

5 TRIGGERING POTENTIAL

As briefly mentioned before, previous studies have suggested that the PGV of the teleseismic surface wave is one of the most important factors in controlling the potential of triggering tremor (Peng *et al.* 2009; Rubinstein *et al.* 2009). However, it is still not clear whether triggering potential also depends on frequency (Brodsky & Prejean 2005; Peng *et al.* 2009; Rubinstein *et al.* 2009; Guilhem *et al.* 2010), incidence angle (Hill 2008; Rubinstein *et al.* 2009; Hill 2010), background tremor rate (Rubinstein *et al.* 2009), background noise (Gomberg 2010) or other factors. In this section, we quantified

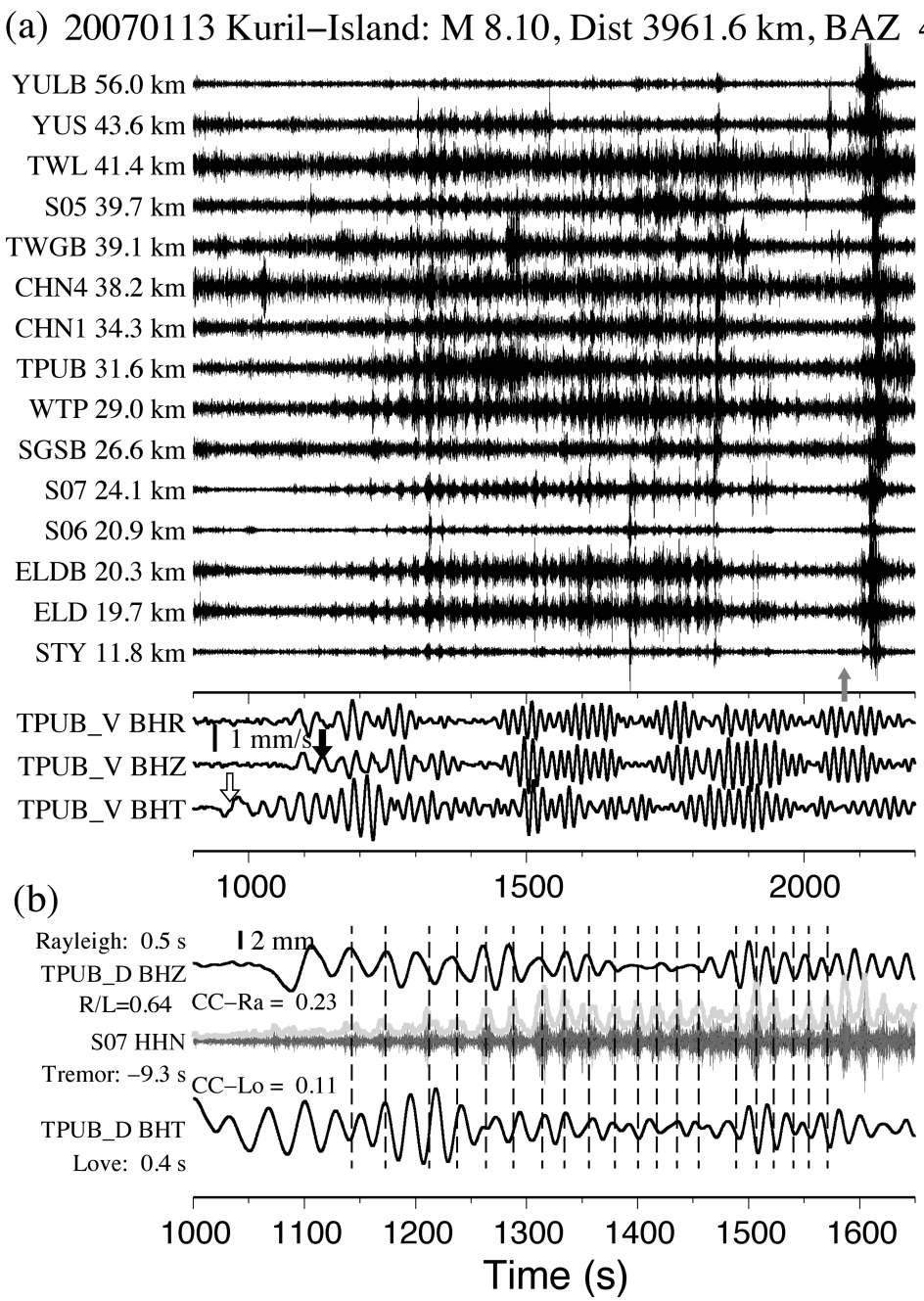

Figure 11. Tremor triggered by the 2007 M_w8.1 Kuril Island earthquake. (a) The 2–8 Hz bandpass-filtered seismograms in the N-component showing the moveout of tremor from the southern CR. The vertical grey arrow marks the origin time of a local earthquake from the CWB catalogue. (b) A detailed comparison between the displacement seismograms at TPUB and bandpass-filtered seismogram at TAIGER station TGS07. Other notations are the same as in Fig. 4.

the triggering threshold in terms of the amplitude (PGV), incidence angle and frequency of the distant surface waves. In addition, we also evaluated the relationship between the amplitudes of the triggering waves and triggered tremors and use them to test the 'clock-advance' model for earthquake triggering (Gomberg 2010) and the role of background noise level on the triggering threshold.

5.1 Amplitude (PGV)

Fig. 2 shows the PGV and the corresponding peak dynamics stress σ_d measured from the transverse (Fig. 2a) and vertical (Fig. 2b) components for all 45 teleseismic earthquakes. To calculate the corresponding dynamic stress σ_d, we used the equation $\sigma_d = G\dot{u}/v_s$ (Jaeger & Cook 1979), where G is the shear modulus, $\dot{u}$ is the PGV and v_s is the phase velocity. For all nine triggering earthquakes, the measured transverse PGV ranges from 0.10 cm s^{-1} to 0.835 cm s^{-1}, which corresponds to the peak dynamic stress of 7.8–61.1 KPa, if we use a nominal shear modulus of 30 GPa and a constant Rayleigh waves velocity of 3.5 km s^{-1} (Miyazawa & Brodsky 2008). The PGV of 0.1 cm s^{-1} appears to separate most of triggering and non-triggering earthquakes in both transverse and vertical components, which corresponds to an apparent tremor-triggering threshold 7–8 KPa. It is worth noting that some events with the transverse PGVs

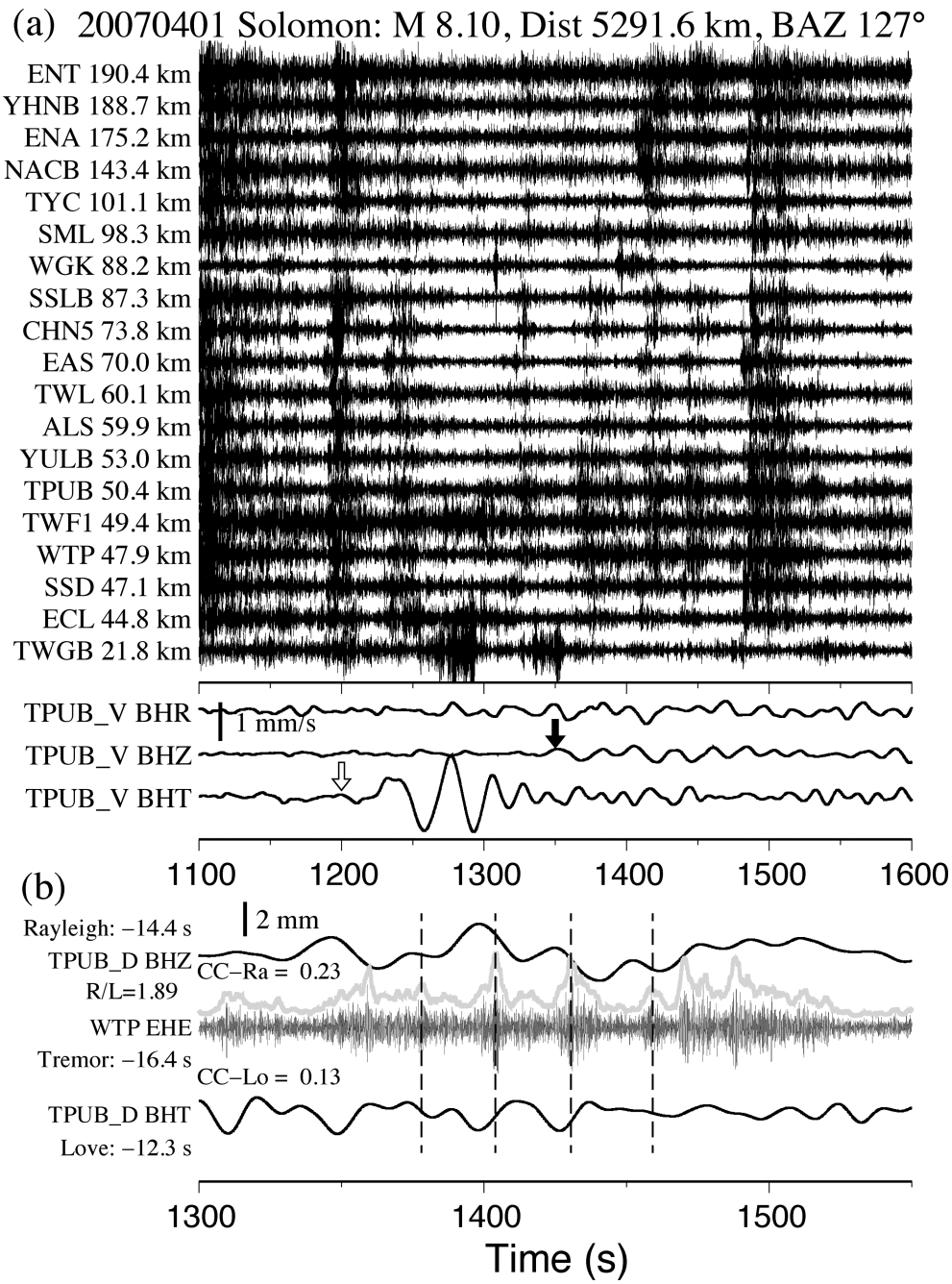

Figure 12. Tremor triggered by the 2007 M_w8.1 Solomon earthquake. (a) The 2–8 Hz bandpass-filtered seismograms in E-component showing the moveout of tremor from the southern CR. (b) A detailed comparison between the displacement seismograms at TPUB and bandpass-filtered seismogram at WTP. Other notations are the same as in Fig. 4.

(Fig. 2a) just above (the 2005 October 8 M_w7.6 Pakistan) or below (the 2006 November 15 M_w8.3 Kuril Island earthquake) the aforementioned threshold did not trigger tremor, while one event (the 2000 June 4 M_w7.9 Sumatra earthquake) just below the threshold is considered as possible triggered tremor. For the vertical component (Fig. 2b), the 2007 M_w8.1 Solomon event with relative low PGV (0.03 cm s^{-1} or 2.4 KPa) below the inferred 0.1 cm s^{-1}, still triggered tremor. Nonetheless, we suggest that the PGV is one of the most important parameters in controlling the trigger thresholds.

5.2 Incidence angle

To examine the triggering potential of surface waves coming from different angles, we modelled the dynamic stress caused by the passage of Love and Rayleigh waves with an arbitrary incident angle on critically stressed faults (Fig. 14) under the Coulomb failure criteria (Hill 2010; Gonzalez-Huizar & Velasco 2011; Wu *et al.* 2011), and then compared the modelling results with our observations. The triggering potential is controlled by the Coulomb failure function that depends on fault types, orientations, incidence angles and types of surface waves.

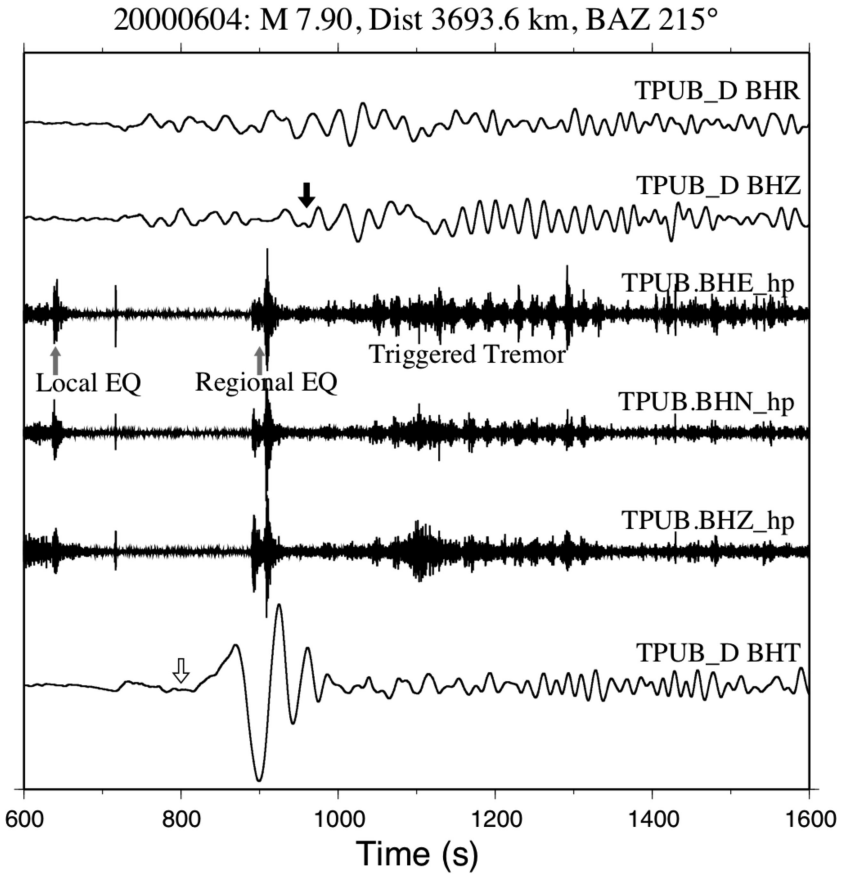

Figure 13. A comparison between the broad-band displacement seismograms and 5 Hz high-pass-filtered seismograms at station TPUB showing possible tremor triggered by the 2000 M_w7.9 Sumatra earthquake. The open and black vertical arrows mark the approximate arrivals of the Love and Rayleigh waves. The grey arrows mark the origin times of local and regional earthquakes.

The modelling procedure generally follows Wu *et al.* (2011) and is briefly described here. We assume tremor was triggered at an average depth of 20 km (Fig. 1b) by the surface waves with 20 s periods. Based on the fault models and slip directions from our previous studies (Peng & Chao 2008; Tang *et al.* 2010), we tested four fault-plane models in different fault types and dipping angles: (1) the high-angle (dip = 60°) reverse (Figs 14b and 15a) and low-angle (dip = 15°) reverse (Figs 14b and 15b) fault models that are parallel to the CR (i.e. strike = N16°E, Suppe 1981), and (2) the high-angle left-lateral (LL) strike-slip (Figs 14c and 15c) and low-angle LL strike-slip (Figs 14c and 15d) models. The triggering potentials for the Love and Rayleigh waves have been normalized assuming comparable displacement amplitudes at the surface for both types of surface waves. Note that the incident angle in Fig. 15 is defined as counter-clockwise (Hill 2010; Wu *et al.* 2011) from the strike of the CR (Fig. 14a), and is different from the definition of backazimuth in Fig. 2.

Here we compared the triggering potential between the four models (Fig. 15) and the observations. The observations are based on the comparison between the tremor bursts and displacement seismograms (panel b of Figs 4–12) and are also summarized in Fig. 14(a). In general, the triggering potential of the models shown in Figs 15(a)–(c) are not consistent with the observations. For instance, both high-angle dip-slip models in Figs 15(a) and (c) suggest that Love waves (red solid line) have higher triggering potential in fault-parallel direction (around 0° and 180°), which is opposite to the observations (i.e. the 1998 Ceram Sea, 2003 Tokachi-Oki, 2004 Sumatra, 2005 Nias, 2007 Kuril Island and 2007 Sumatra earthquakes show predominate Rayleigh-wave triggering). In fault-normal direction (around 90° and –90°), the model of Fig. 15c is consistent with the Love-wave triggering of the 2001 Kunlun earthquake, but not for the same case shown in Fig. 15(a). As for the model with low-angle reverse faulting (Fig. 15b), the Rayleigh wave (blue dashed line) has highest triggering potential for all incidence angles, which is not consistent with the observations.

On the other hand, the model of Fig. 15(d) (LL faulting on the low-angle fault) has 77.8 per cent (seven out of nine) of triggering earthquakes that are consistent with the observations. In detail, one out of three of earthquakes in fault-normal direction show Love-wave triggering (i.e. the 2001 Kunlun earthquake in red colour). In fault-parallel direction, all six events are triggered by Rayleigh wave. However, not all triggering events are consistent with this model prediction. For example, the 2007 Solomon and 2008 Wenchuan earthquakes correlate better with Rayleigh waves. We additionally tested different dipping angles of this model and found similar triggering potential within 15° and 45°. Hence, we suggest that the low-to-median dipping angle of LL strike-slip fault model (Figs 14c and 15d) better explains the observations.

5.3 Frequency

In this section we quantified the triggering threshold in terms of frequency by computing the amplitude spectra of surface waves

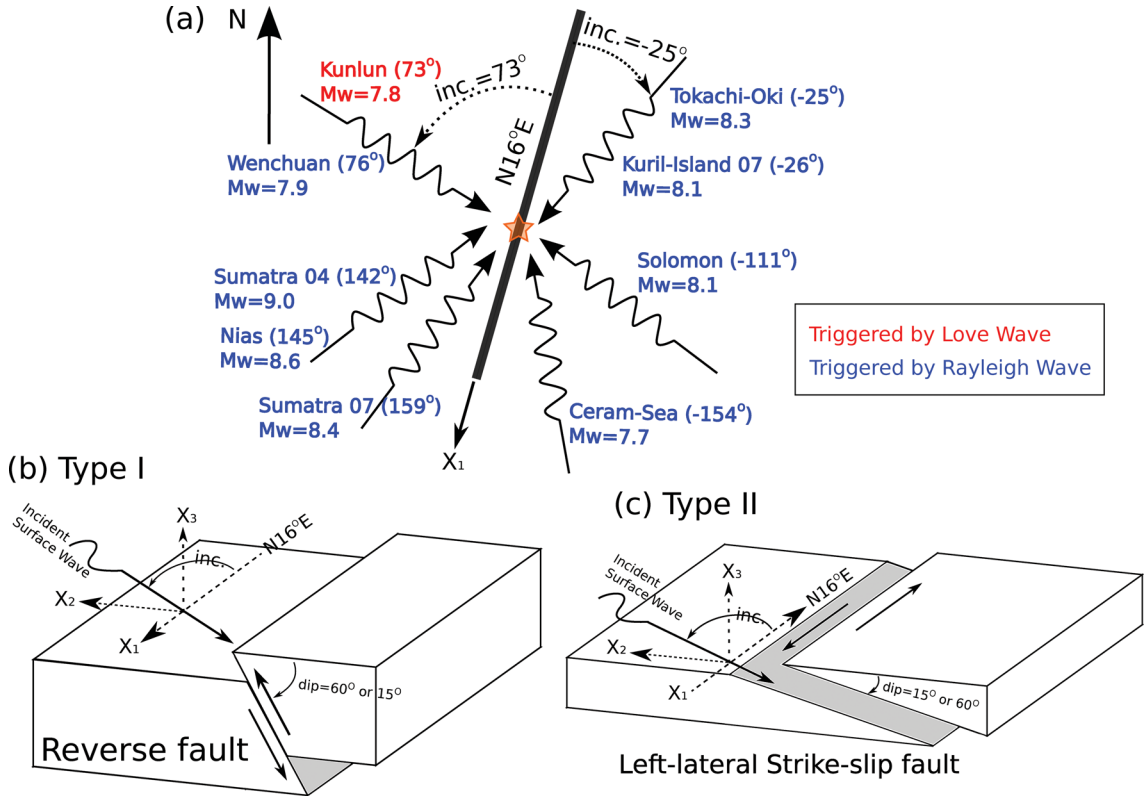

Figure 14. Schematic diagram showing multiple tremor source models. (a) A map view of the strike of the Central Range (N16°E), and the incidence angles of the nine tremor triggering earthquakes. The events that show triggering with the Love and Rayleigh types of waves are marked in red and blue colours, respectively. (b) Type I: A reverse fault model with high- or low- (60° or 15°) dipping angles. (c) Type II: A low-angle oblique-slip fault plane model with high or low dipping angles.

for all 45 teleseismic earthquakes recorded at TPUB. The analysis procedure generally follows that of Peng *et al*. (2009) and is briefly described here. We first cut the instrument-corrected velocity seismograms within the apparent velocity of 5–2 km s^{-1} to include most of the surface waves. Next, we compute the corresponding spectra for both the transverse and vertical components and smooth the resulting spectra with a sliding window of 10 points. Fig. 16 shows the velocity spectra for the nine triggering (colour lines), one possibly triggering (black line) and 35 non-triggering (grey lines) earthquakes in the transverse (a) and vertical (b) components. The surface wave spectra of these triggering earthquakes are mainly peaked in the frequency range from 10 to 50 s (0.02–0.1 Hz), and appear to be on the top of those non-triggering earthquakes, although there is no clear separation between these triggering and non-triggering groups (Peng *et al.* 2009).

Previous studies have suggested that the surface waves longer than 30 s are more efficient in triggering tremor (Guilhem *et al.* 2010) and earthquakes (Brodsky & Prejean 2005). To better quantify the relationship between the frequency contents of the surface waves and triggered tremor, we filtered the displacement seismograms into long-period (>30 s), intermediate-period (30–10 s), and short-period (10–1 s) ranges, then compared them with tremor bursts for all nine triggering events. Fig. 17 shows three representative examples of such comparisons in different frequency ranges. For the Kunlun triggering case, the tremor bursts appear to be initiated by or show better correlation with the long-period Love or Rayleigh waves. For the Nias and the Tokachi-Oki cases, the tremor bursts do not show a clear correlation with the long-period Love wave, but are modulated later by the intermediate-period Rayleigh waves. Such a difference could be partially caused by the excitations of long- or intermediate-periods surface waves due to different styles of main shock faulting. Nevertheless, here we show that intermediate-period surface waves could trigger/modulate tremor and long-period signals are not always needed.

To test this statement further, we evaluate the triggering potential by measuring the PGVs from long-, intermediate- and short-periods surface waves. As shown in Fig. 18(b)–(c), the PGVs from the intermediate-period surface waves appear to better separate the triggering/non-triggering cases than the long- or short-period surface waves. This is different than the results of Guilhem *et al.* (2010), who found that long-period surface waves (>30 s) better separate the triggering/non-triggering groups around Parkfield. It is worth noting that the intermediate-period (30–10 s) signals in this study include the predominant 20 s surface waves (i.e. spectral peaks in Fig. 16). Hence, the apparent associations between the triggered tremor and intermediate-period surface waves could also be explained by the amplitude difference in different frequency bands.

5.4 Testing of the 'clock-advance' model and background noise level

Assuming tremor occurs on the fault patches that are close to failure, Gomberg (2010) proposed the 'clock-advance' model to explain the phenomenon of triggered tremors. In this model, triggered tremor can be considered as a sped-up occurrence of ambient tremor under fast loading from the passing surface waves. Because the rate of altered failure (i.e. triggered tremor) is directly proportional to

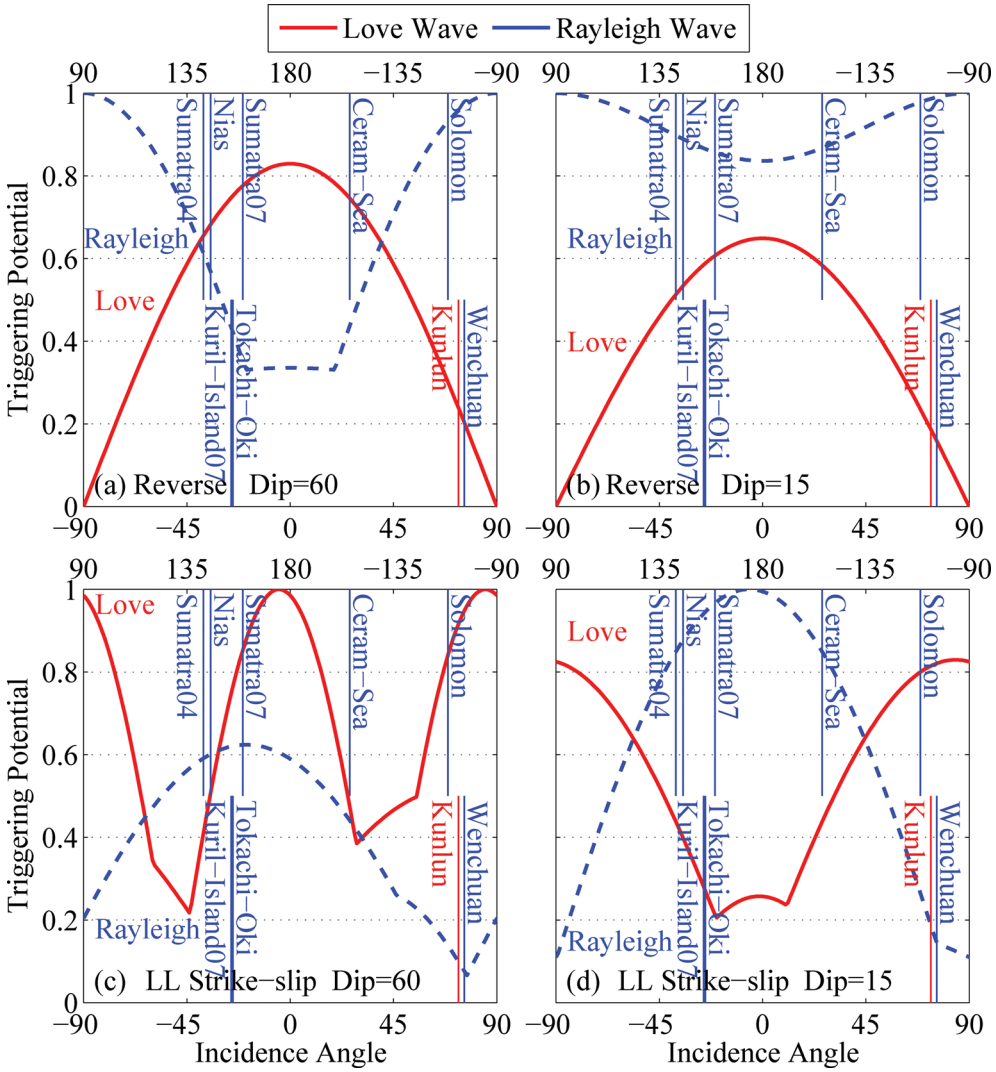

Figure 15. (a, b) Triggering potential of the reverse fault model dipping at 60° and 15° (Fig. 14b). (c, d) Triggering potential of the left-lateral (LL) strike-slip fault model dipping at 60° and 15° (Fig. 14c). The triggering potentials of the Love (red solid line) and Rayleigh (blue dashed line) waves are calculated with 20 s period surface waves at a depth of 20 km assuming the coefficient of friction $\mu = 0.2$ and comparable displacement amplitudes at the surface for both Love and Rayleigh waves. The vertical solid lines mark the incidence angle of the nine triggering earthquakes. The red and blue colours mark the events that show triggering with the Love and Rayleigh waves, respectively.

the background (i.e. ambient tremor) rate and the amplitude of the triggering wave, we would expect to see higher likelihood of triggering with greater ambient rate, and larger amplitude of triggered tremor signals with larger amplitude of triggering waves (Miyazawa & Brodsky 2008). Gomberg (2010) used four observations of triggered tremor in Cascadia (Rubinstein *et al.* 2009) and found that they could not be simply explained by the 'clock-advance' model.

Because the ambient tremor observation around our study region is still in the developing stage (Chao *et al.* 2010), here we only quantified the relationship between the surface wave amplitude and the amplitude of triggered tremor. We measured the median amplitudes of 2–8 Hz bandpass-filtered envelope functions recorded at two horizontal components of station TPUB during the surface waves for all triggering and non-triggering events. In addition, we calculated the median background noise levels for individual event from the envelope functions during the 600 s time period before the occurrence of each main shock. The median, rather than the maximum or average values in the 2–8 Hz envelope functions are used here to avoid potential contaminations from impulsive local earthquakes or other transient high-frequency noises. We found a relatively strong correlation (with a CC of 0.90) for the nine triggering and one possible-triggering events between the triggered tremor amplitudes and surface waves amplitudes (Fig. 19a). Such a correlation is generally consistent with the 'clock-advance' model (Gomberg 2010). In comparison, there is no clear correlation between maximum surface waves amplitude and 2–8 Hz energy during the surface waves for the 35 non-triggering events (with a CC of 0.06). The median noise level for all events (shadow area) is about 20 nm s^{-1}, which is a factor of 2 below the minimum tremor amplitude of ∼40 nm s^{-1} observed in this study (Fig. 19a).

Fig. 19(b) shows the SNRs for all events. In general, the SNRs of the nine triggering events and one possible-triggering event are greater than 2, but do not show a simple linear relationship with the surface wave amplitudes. This is likely because the background noise levels for these events vary significantly. For the 35 non-triggering events, only three events (i.e. the 2001 January 1 M_w7.5, the 2006 April 20 M_w7.6 and 2007 January 21 M_w7.5 earthquakes) have SNR larger than 2. The high-frequency signals during

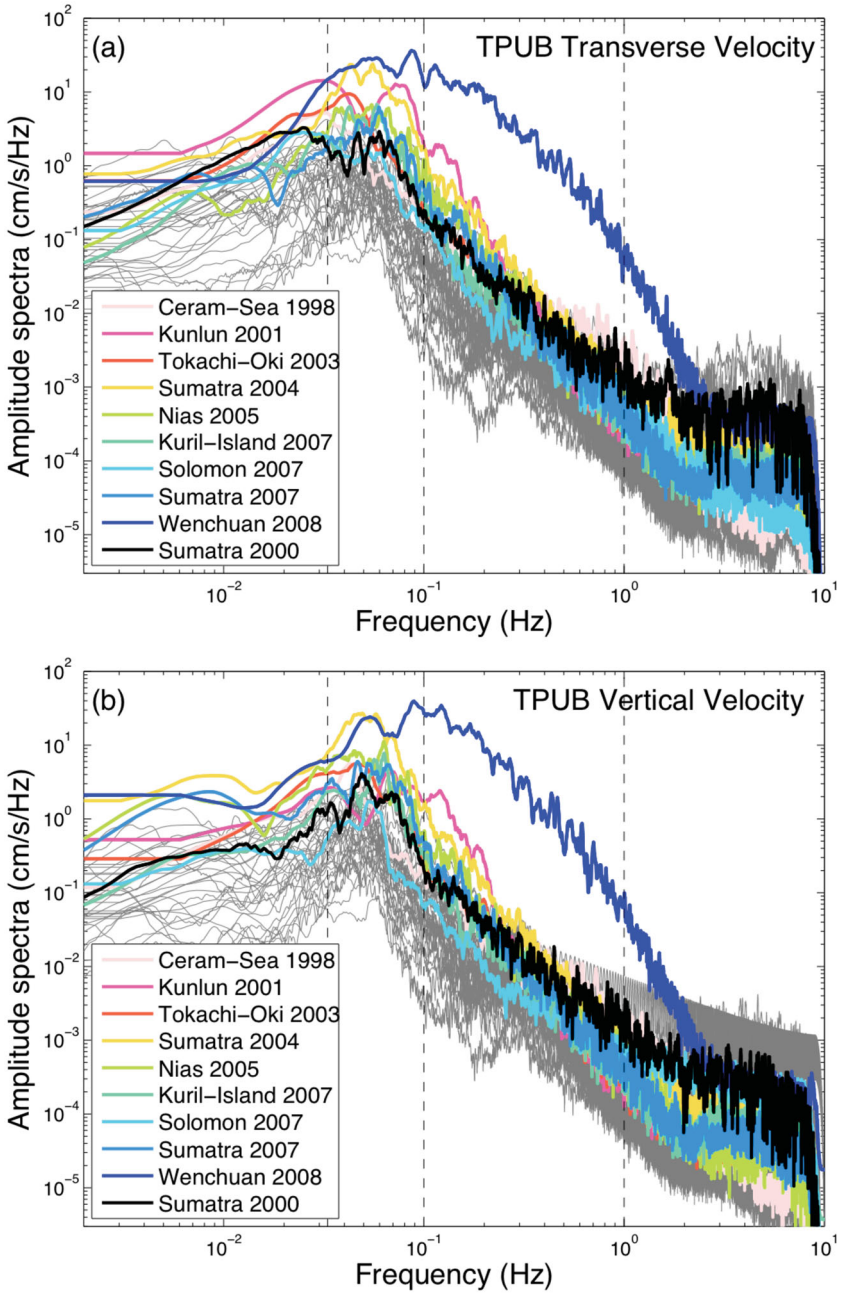

Figure 16. Velocity spectra for nine triggering earthquakes (colour lines), one possible triggering earthquake (in black line) and non-triggering earthquakes (grey lines) in the transverse (a) and vertical (b) components at the broad-band station TPUB. The vertical dashed lines mark the frequencies corresponding to 0.033 Hz (30 s), 0.1 Hz (10 s) and 1 Hz (1 s).

surface waves of these events do not have the characteristics of triggered tremor (i.e. modulated high-frequency bursts that are coherent among nearby stations), and hence the sources of such high-frequency signals are unclear to us at this stage. In addition, we note that the amplitudes of two non-triggering events with PGVs larger than the aforementioned threshold of 0.1 cm s^{-1} have SNR less than 2. It is possible that these events could have triggered tremors with amplitudes smaller than the level of background noise, which prevent them from being identified as tremor triggering events. Nevertheless, it is reasonable to assume that an SNR of 2 is needed for the triggered tremor to be visually identified in this study. This number is close to the aforementioned median noise level of 20 nm s^{-1}, and the minimum tremor amplitude of ~40 nm s^{-1}. In other words, we suggest that the background noise level could play an important role in determining the smallest triggered tremor observed in this study.

6 DISCUSSIONS AND CONCLUSIONS

In this study we have identified nine teleseismic earthquakes that triggered clear tremors beneath the CR. In general, tremors from the southern CR are located between the CLF and the LVF (Peng & Chao 2008; Tang *et al.* 2010) below the seismogenic zone (Fig. 1b) and above the Moho depth calculated by receiver functions (Tang *et al.* 2011). The nine tremor locations in the south (Figs 1 and 3)

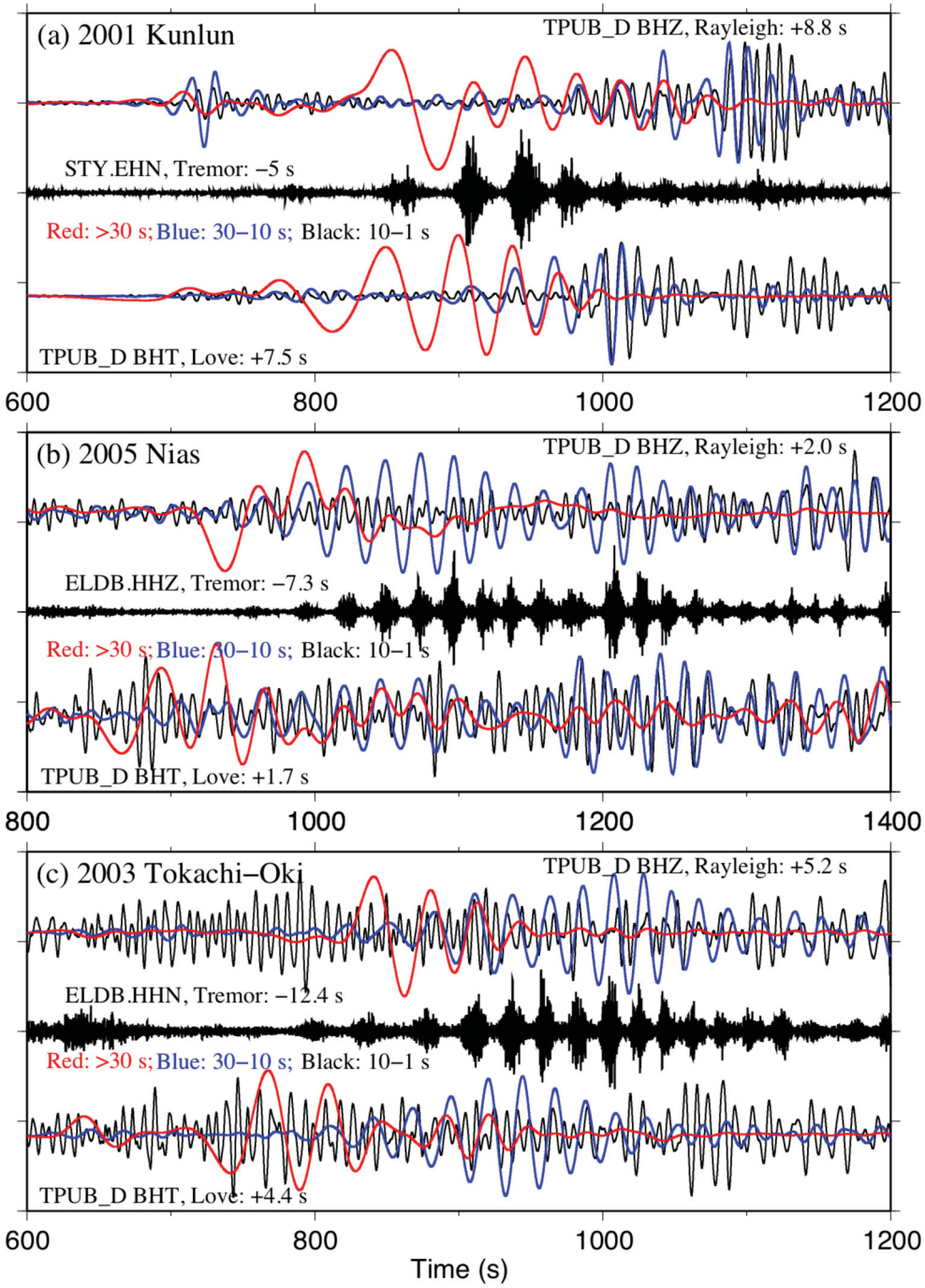

Figure 17. Comparisons between tremor and different periods of surface waves for the (a) 2001 Kunlun, (b) 2005 Nias and (c) 2003 Tokachi-Oki earthquakes. The long-period (>30 s), intermediate-period (30–10 s) and short-period (10–1 s) surface waves are marked as red, blue and black colours, respectively. All displacement seismograms have been normalized to the same scale and time-shifted back to the tremor source region.

were close to the tremor source triggered by the 2001 M_w7.8 Kunlun earthquake (Peng & Chao 2008). In addition, those locations are roughly centred around those of the LFEs triggered by the 2005 Nias earthquake (Tang *et al.* 2010), although the hypocentral depth of 15–25 km for most events shown in this study is on the top of the LFEs distributed between 12 and 38 km (Fig. 1b). Such a difference could be mainly caused by the envelope-based technique in this study with only the *S*-wave information, and the LFE-based technique in Tang *et al.* (2010) with both the *P* and *S* arrivals, which provides better constraints on the depth and tends to place the hypocentres at larger depth than other techniques (Kao *et al.* 2009; La Rocca *et al.* 2009). Other five tremor locations are distributed around the northern CR (Fig. 1a). However, the tremor locations in that region have larger uncertainties (see Table S3) due to lack of sufficient seismic recordings. Further studies are needed to better constrain the hypocentral locations in the northern CR.

The apparent triggering threshold obtained in this study is about ∼0.1 cm s^{-1} PGVs, which corresponds to the peak dynamic stress of 7–8 KPa (Fig. 2). This number is slightly higher than the 2–3 KPa threshold found in a similar study of triggered tremor along the

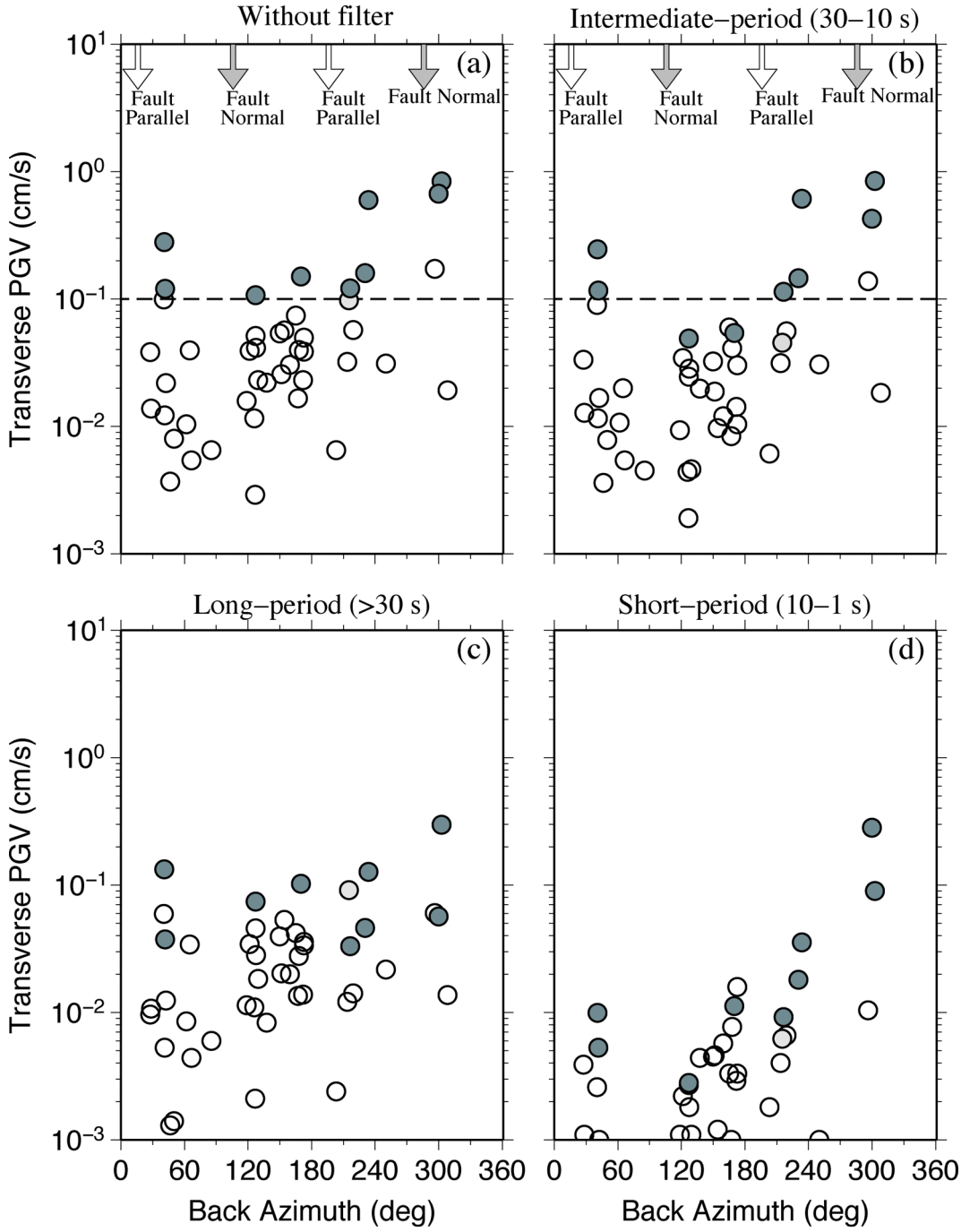

Figure 18. PGV versus backazimuth in transverse component for different frequency bands: (a) without filter, (b) intermediate-period (30–10 s), (c) long-period (>30 s) and (d) short-period (10–1 s) ranges. Other notations are the same as in Fig. 2.

Parkfield section of SAF in central California (Peng *et al.* 2009). However, we found that the triggering threshold could be partially controlled by the background noise level (Fig. 19). This is consistent with our recent study by comparing triggered tremor in three regions in California (Chao *et al.* 2011). Hence, the subtle difference between Taiwan and Parkfield could be related to the use of surface stations in Taiwan and more sensitive and less noisy borehole stations at Parkfield. In addition, we found a positive relationship between the amplitudes of the triggering surface waves and the amplitudes of the triggered tremor, which are consistent with the prediction by the 'clock-advance' model (Gomberg 2010). Therefore, we suggest that surface waves with relatively smaller amplitudes could also have the potential of triggering weaker tremors, although they may not be easily observed if their amplitudes are near or below the background noise level. In addition to the amplitudes, we also found that the incidence angles (Figs 2 and 15) and the frequency contents (Figs 16–18) could also play some roles in controlling the triggering potential. In particular, we found that the intermediate-period (30–10 s) surface waves appear to dominate the triggering potential. This is slightly different than the previous observations of long-period (>30 s) surface waves being the most important in triggering tremor (Guilhem *et al.* 2010)

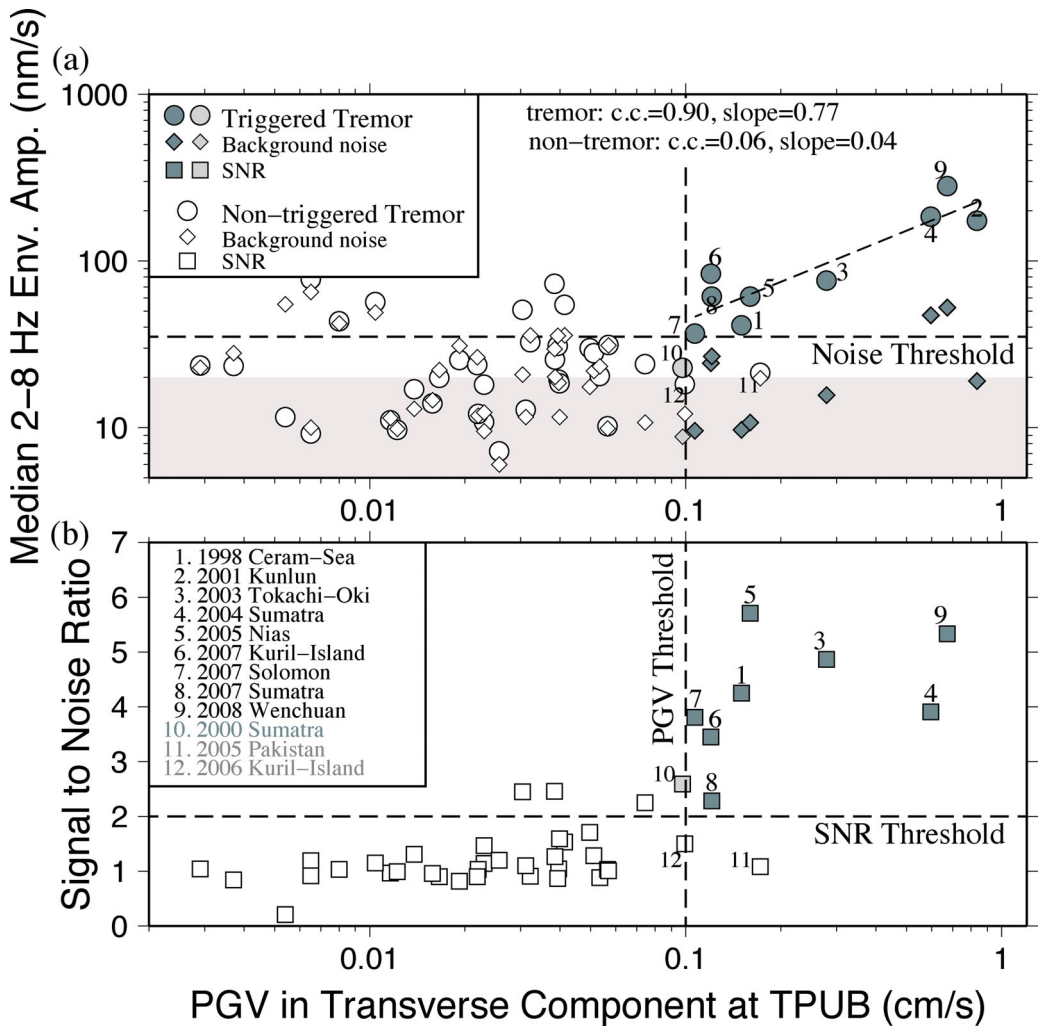

Figure 19. Maximum surface wave amplitude (horizontal axis) versus (a) median amplitude of the 2–8 Hz bandpass-filtered envelope functions during the surface waves and (b) signal-to-noise ratio (SNR) measured at station TPUB. The background noise level of each event is calculated from a 600 s time window before the occurrence of each main shock. The data points associated with the nine tremor triggering, one possible triggering and 35 non-tremor triggering events are marked as solid, grey and open symbols. The vertical dashed lines show the apparent triggering amplitude threshold of ∼0.1 cm s^{-1}. The horizontal dashed line in (a) marks the apparent triggering background noise threshold of ∼35 nm s^{-1}. The light grey background shows the median noise level for all events. The horizontal dashed line in (b) marks the SNR of 2.

and microearthquakes (Brodsky & Prejean 2005). We suggest that long-period waves are helpful, but are not required in long-range triggering.

We found that both Love and Rayleigh waves are capable of triggering tremors in the CR (Figs 4–12). In particular, tremors show better correlations with Rayleigh waves for strike-parallel incidence (Fig. 14a). Only one case shows Love-wave triggering for strike-normal incidence (Fig. 4). These observations are consistent with those by Velasco *et al.* (2009), and can be qualitatively explained by left-lateral shear slip on an low-angle detachment fault (Fig. 14c). This is the same model originally proposed by Peng & Chao (2008), but is inconsistent with the distributions of triggered LFEs (Fig. 1b) that are interpreted to occur on the high-angle reverse CLF (Tang *et al.* 2010). Because the tremor locations (and especially the depth) obtained from this study have large uncertainties, we could not use them to further constrain the fault-dipping angle. Systematic relocations of tremors (Ide 2010) and LFEs (Shelly & Hardebeck 2010), together with the focal mechanisms (Ide *et al.* 2007) and polarization analysis (Wech & Creager 2007; Miyazawa & Brodsky 2008) of the triggered and ambient tremors are needed to better understand the fault motions that are responsible for generating tremor signals beneath the CR.

ACKNOWLEDGMENTS

We thank the Institute of Earth Sciences in Academia Sinica and the Central Weather Bureau for providing seismic data used in this study. We also thank Chau-Huei Chen for providing TAIGER network data. The manuscript benefited from valuable comments by Joan Gomberg, Justin Rubinstein, Yih-Min Wu and two anonymous reviewers. This study is supported by the National Science Foundation (EAR-0809834 and EAR-0956051).

REFERENCES

Beroza, G.C. & Ide, S., 2009. Deep tremors and slow quakes, *Science*, **324**, 1025–1026, doi:10.1126/science.1171231.

Beroza, G.C. & Ide, S., 2011. Slow earthquakes and nonvolcanic tremor, *Annu. Rev. Earth planet. Sci.*, **39**, 271–296, doi:10.1146/annurev-earth-040809-152531.

Brodsky, E.E. & Prejean, S.G., 2005. New constraints on mechanisms of remotely triggered seismicity at Long Valley Caldera, *J. geophys. Res.*, **110**, B04302, doi:10.1029/2004JB003211.

Brown, J.R. *et al*., 2009. Deep low-frequency earthquakes in tremor localize to the plate interface in multiple subduction zones, *Geophys. Res. Lett.*, **36**, L19306, doi:10.1029/2009GL040027.

Chao, K., Peng, Z., Tang, C.-C., Lin, C.-H. & Chen, C.H., 2010. Deep tremor activities beneath the central range in Taiwan and their relationship to local, regional, and teleseismic earthquakes, *EOS, Trans. Am. geophys. Un.*, **91**(50), Fall Meet. Suppl., Abstract S23A-2106.

Chao, K., Peng, Z., Fabian, A. & Ojha, L., 2011. Comparisons of triggered tremor in California, *Bull. seism. Soc. Am*, in press.

Fry, B., Chao, K., Bannister, S. & Peng, Z., 2011. Deep tremor beneath the Hikurangi margin in New Zealand triggered by the 2010 Mw 8.8 Chile earthquake, *Geophys. Res. Lett*, **38**, L15306, doi:10.1029/2011GL048319.

Ghosh, A., Vidale, J.E., Peng, Z., Creager, K.C. & Houston, H., 2009. Complex nonvolcanic tremor near Parkfield, California, triggered by the great 2004 Sumatra earthquake, *J. geophys. Res.*, **114**, B00A15, doi:10.1029/2008JB006062.

Gomberg, J., 2010. Lessons from (triggered) tremor, *J. geophys. Res.*, **115**, B10302, doi:10.1029/2009JB007011.

Gomberg, J., Rubinstein, J.L. & Peng, Z., 2008. Widespread triggering of nonvolcanic tremor in California, *Science*, **319**, 173, doi:10.1126/science.1149164.

Gonzalez-Huizar, H. & Velasco, A.A., 2011. Dynamic triggering: stress modeling and a case study, *J. geophys. Res*, **116**, B02304, doi:10.1029/2009JB007000.

Guilhem, A., Peng, Z. & Nadeau, R.M., 2010. High-frequency identification of non-volcanic tremor triggered by regional earthquakes, *Geophys. Res. Lett*, **37**, L16309, doi:10.1029/2010GL044660.

Hill, D., 2008. Dynamic stresses, Coulomb failure, and remote triggering, *Bull. seism. Soc. Am*, **98**(1), 66–92, doi:10.1785/0120070049.

Hill, D.P., 2010. Surface-wave potential for triggering tectonic (non-volcanic) tremor, *Bull. seism. Soc. Am*, **100**(5A), 1859–1878, doi:10.1785/0120090362.

Ide, S., 2010. Striations, duration, migration and tidal response in deep tremor, *Nature*, **466**(7304), 356–359, doi:10.1038/nature09251.

Ide, S., Shelly, D. & Beroza, G.C., 2007. Mechanism of deep low frequency earthquakes: further evidence that deep non-volcanic tremor is generated by shear slip on the plate interface, *Geophys. Res. Lett.*, **34**, L03308, doi:10.1029/2006GL028890.

Jaeger, J.C. & Cook, N.G.W., 1979. *Fundamentals of Rock Mechanics*, 3rd edn, Chapman and Hall, New York, NY.

Jiang, T., Peng, Z., Wang, W. & Chen, Q.-F., 2010. Remotely triggered seismicity in Continental China by the 2008 Mw7.9 Wenchuan earthquake, *Bull. seism. Soc. Am*, **100**(5B), 5274–5289, doi:10.1785/0120090286.

Kao, H., Shan, S.-J., Dragert, H. & Rogers, G., 2009. Northern Cascadia episodic tremor and slip: A decade of tremor observations from 1997 to 2007, *J. geophys. Res*., **114**, B00A12, doi:10.1029/2008JB006046.

La Rocca, M., Galluzzo, D., Malone, S., McCausland, W. & Del Pezzo, E., 2010. Array analysis and precise source location of deep tremor in Cascadia, *J. geophys. Res.*, **115**, doi:10.1029/2008JB006041.

Liu, C., Linde, A.T. & Sacks, I.S., 2009. Slow earthquakes triggered by typhoons, *Nature*, **459**, 833–836, doi:10.1038/nature08042.

Miyazawa, M. & Brodsky, E., 2008. Deep low-frequency tremor that correlates with passing surface waves, *J. geophys. Res.*, **113**, B01307, doi:10.1029/2006JB004890.

Miyazawa, M. & Mori, J., 2005. Detection of triggered deep low-frequency events from the 2003 Tokachi-oki earthquake, *Geophys. Res. Lett.*, **32**, L10307, doi:10.1029/2005GL022539.

Miyazawa, M. & Mori, J., 2006. Evidence suggesting fluid flow beneath Japan due to periodic seismic triggering from the 2004 Sumatra-Andaman earthquake, *Geophys. Res. Lett.*, **33**, L05303, doi:10.1029/2005GL025087.

Miyazawa, M., Brodsky, E. & Mori, J., 2008. Learning from dynamic triggering of low-frequency tremor in subduction zones, *Earth Planets Space*, **60**, e17–e20.

Nadeau, R.M. & Dolenc, D., 2005. Nonvolcanic tremors deep beneath the San Andreas fault, *Science*, **307**, 389, doi:10.1126/science.1107142.

Obara, K., 2002. Nonvolcanic deep tremor associated with subduction in southwest Japan, *Science*, **296**, 1679–1681, doi:10.1126/science.1070378.

Obara, K. & Hirose, H., 2006. Non-volcanic deep low-frequency tremors accompanying slow slips in the southwest Japan subduction zone, *Tectonophysics*, **417**, 33–51, doi:10.1016/j.tecto.2005.04.013.

Outerbridge, K.C. *et al*., 2010. A tremor and slip event on the Cocos-Caribbean subduction zone as measured by a global positioning system (GPS) and seismic network on the Nicoya Peninsula, Costa Rica, *J. geophys. Res.*, **115**, B10408, doi:10.1029/2009JB006845.

Payero, J.S., Kostoglodov, V., Shapiro, N., Mikumo, T., Iglesias, A., Perez-Campos, X. & Clayton, R.W., 2008. Nonvolcanic tremor observed in the Mexican subduction zone, *Geophys. Res. Lett.*, **35**, L07305, doi:10.1029/2007GL032877.

Peng, Z. & Chao, K., 2008. Non-volcanic tremor beneath the Central Range in Taiwan triggered by the 2001 Mw7.8 Kunlun earthquake, *Geophys. J. Int.*, **175**(2), 825–829, doi:10.1111/j.1365-246X.2008.03886.x.

Peng, Z. & Gomberg, J., 2010. An integrated perspective of the continuum between earthquakes and slow-slip phenomena, *Nature Geosci.*, **100**, 5274–5289.

Peng, Z., Vidale, J.E., Creager, K.C., Rubinstein, J.L., Gomberg, J. & Bodin, P., 2008. Strong tremor near Parkfield, CA, excited by the 2002 Denali Fault earthquake, *Geophys. Res. Lett.*, **35**, L23305, doi:10.1029/2008GL036080.

Peng, Z., Vidale, J.E., Wech, A.G., Nadeau, R.M. & Creager, K.C., 2009. Remote triggering of tremor along the San Andreas Fault in central California, *J. geophys. Res.*, **114**, B00A06, doi:10.1029/2008JB006049.

Peng, Z., Hill, D.P., Shelly, D.R. & Aiken, C., 2010a. Remotely triggered microearthquakes and tremor in central California following the 2010 Mw8.8 Chile Earthquake, *Geophys. Res. Lett.*, **37**, L24312, doi:10.1029/2010GL045462.

Peng, Z., Wang, W., Chen, Q.-F. & Jiang, T., 2010b. Remotely triggered seismicity in northeast China following the 2008 Mw7.9 Wenchuan earthquake, *Earth Planets Space*, **62**, 893–898, doi:10.5047/eps.2009.03.00.

Peterson, C. & Christensen, D., 2009. Possible relationship between nonvolcanic tremor and the 1998–2001 slow slip event, south central Alaska, *J. geophys. Res.*, **114**, B06302, doi:10.1029/2008JB006096.

Rogers, G. & Dragert, H., 2003. Episodic tremor and slip on the Cascadia Subduction zone: the chatter of silent slip, *Science*, **300**, 1942–1943.

Rubinstein, J.L., Vidale, J.E., Gomberg, J., Bodin, P., Creager, K.C. & Malone, S.D., 2007. Non-volcanic tremor driven by large transient shear stresses, *Nature*, **448**, 579–582.

Rubinstein, J.L., Gomberg, J., Vidale, J.E., Wech, A.G., Kao, H., Creager, K.C. & Rogers, G., 2009. Seismic wave triggering of nonvolcanic tremor, episodic tremor and slip, and earthquakes on Vancouver Island, *J. geophys. Res.*, **114**, B00A01, doi:10.1029/2008JB005875.

Rubinstein, J.L., Shelly, D.R. & Ellsworth, W.L., 2010. Non-volcanic tremor: a window into the roots of fault zones, in *New Frontiers in Integrated Solid Earth Sciences*, pp. 287–314, eds Cloetingh, S. & Negendank, J., Springer, Berlin, doi:10.1007/978-90-481-2737-5_8.

Schwartz, S.Y. & Rokosky, J.M., 2007. Slow slip events and seismic tremor at circum-Pacific subduction zones, *Rev. Geophys.*, **45**(3), doi:10.1029/2006RG000208.

Shearer, P.M., 1999. *Introduction to Seismology*, Cambridge University Press, Cambridge.

Shelly, D.R., 2009. Possible deep fault slip preceding the 2004 Parkfield earthquake, inferred from detailed observations of tectonic tremor, *Geophys. Res. Lett.*, **36**, L17318, doi:10.1029/2009GL039589.

Shelly, D.R., 2010. Migrating tremors illuminate complex deformation beneath the seismogenic San Andreas fault, *Nature*, **463**, 648–652, doi:10.1038/nature08755.

Shelly, D.R. & Hardebeck, J.L., 2010. Precise tremor source locations and amplitude variations along the lower-crustal central San Andreas Fault, *Geophys. Res. Lett.*, **37**, L14301, doi:14310.11029/12010GL043672, doi:10.1029/2010GL043672.

Shelly, D.R., Beroza, G.C. & Ide, S., 2007. Non-volcanic tremor and low-frequency earthquake swarms, *Nature*, **446**(7133), 305–307, doi:10.1038/nature05666.

Shelly, D.R., Peng, Z., Hill, D.P. & Aiken, C., 2011. Triggered creep as a possible mechanism for delayed dynamic triggering of tremor and earthquakes, *Nature Geosci*, **4**, 384–388.

Shin, T. & Teng, T.-L., 2001. An overview of the 1999 Chi-Chi, Taiwan, earthquake, *Bull. seism. Soc. Am*, **91**(5), 895–913.

Suppe, J., 1981. Mechanics of mountain building and metamorphism in Taiwan, *Mem. Geol. Soc. China*, **4**, 67–89.

Tang, C.-C., Peng, Z., Chao, K., Chen, C.-H. & Lin, C.-H., 2010. Detecting low-frequency earthquakes within non-volcanic tremor in southern Taiwan triggered by the 2005 Mw8.6 Nias earthquake, *Geophys. Res. Lett.*, **37**, L16307, doi:10.1029/2010GL043918.

Tang, C.-C., Zhu, L., Chen, C.-H. & Teng, T.-L., 2011. Significant crustal variation across the Chaochou fault, southern Taiwan: new tectonic implications for convergent plate boundary, *J. Asian Earth Sci.*, **41**(6), 564–570, doi:10.1016/j.jseaes.2010.12.00.

Velasco, A.A., Gonzalez-Huizar, H. & Hernandez, S., 2009. Dynamic stress modeling for the triggering of non-volcanic tremors, *EOS, Trans. Am. geophys. Un.*, **90**(52), Fall Meet. Suppl., Abstract T11C-1820.

Wech, A. & Creager, K., 2007. Cascadia tremor polarization evidence for plate interface slip, *Geophys. Res. Lett.*, **34**(L2)2306, doi:10.1029/2007GL031167.

West, M., Sanchez, J. & McNutt, S., 2005. Periodically triggered seismicity at Mount Wrangell, Alaska, after the Sumatra earthquake, *Science*, **308**(5725), 1144–1146.

Wu, Y.-M., Chang, C.-H., Zhao, L., Shyu, J.B.H., Chen, Y.-G., Sieh, K. & Avouac, J.-P., 2007. Seismic tomography of Taiwan: improved constraints from a dense network of strong motion stations, *J. geophys. Res.*, **112**, B08312, doi:10.1029/2007JB004983.

Wu, C., Peng, Z., Wang, W. & Chen, Q.-F., 2011. Dynamic triggering of shallow earthquakes near Beijing, China, *Geophys. J. Int.*, **185**, 1321–1334, doi:10.1111/j.1365-246X.2011.05002.x.

Yeh, T.-C., 2011. Dynamic triggering of earthquakes and tremors in Taiwan, *MSc thesis*, National Taiwan University, Taipei.

Yu, S., Chen, H. & Kuo, L., 1997. Velocity field of GPS stations in the Taiwan area, *Tectonophysics*, **274**, 41–59.

SUPPORTING INFORMATION

Additional Supporting Information may be found in the online version of this article:

Table S1. List of all information for 45 teleseismic earthquakes used in this study.

Table S2. (a) Velocity model used to locate tremor sources in the southern Central Range. This is the same velocity model used by Tang *et al.* (GRL, 2010) to locate LFEs in the same region. (b) Velocity model used to locate tremor sources in the northern Central Range.

Table S3. Measured parameters for nine tremor-triggering events used in Figs 1–12 and 19.

Please note: Wiley-Blackwell are not responsible for the content or functionality of any supporting materials supplied by the authors. Any queries (other than missing material) should be directed to the corresponding author for the article.